

## Toward a Theoretical Understanding of the Corrosion Inhibitive Performance on Iron Surface by Some Macrocyclic Polyether Compounds Containing 1, 3, 4-thiadiazole Entity

A. Mahsoun<sup>1</sup>, K. Sadik<sup>1</sup>, M. Elalaoui Belghiti<sup>1</sup>, I. Bahadur<sup>3,4</sup>, A. Aboulmouhajir<sup>1,2,\*</sup>

<sup>1</sup> Team of Molecular Modelling and Spectroscopy, Sciences Faculty, Chouaib Doukkali University, Morocco

<sup>2</sup> Organic synthesis, Extraction and Valorization laboratory, Team of Extraction, Spectroscopy and Valorization, Sciences Faculty of Ain Chock, Hassan II University, Morocco

<sup>3</sup> Department of Chemistry, School of Physical and Chemical Sciences, Faculty of Natural and Agricultural Sciences, North-West University (Mafikeng Campus), Private Bag X2046, Mmabatho 2735, South Africa

<sup>4</sup> Material Science Innovation & Modelling (MaSIM) Focus Area, Faculty of Natural and Agricultural Sciences, North-West University (Mafikeng Campus), Private Bag X2046, Mmabatho 2735, South Africa

\*E-mail: [aboulmouhajir@gmail.com](mailto:aboulmouhajir@gmail.com)

Received: 30 April 2018 / Accepted: 7 July 2018 / Published: 5 August 2018

---

The corrosion inhibitive performance, in acidic medium, of macrocyclic polyether compounds: 1-MCTH, 2-MCTH and their protonated forms, was studied on the basis of their degree of planarity, global and local electronic properties as well as their deformation capacity to adhere the metal surface, by using DFT calculations and Dynamic Monte Carlo simulations. The proton affinity evaluation locates the most favourable site of protonation. 2-MCTH was found more reactive in vacuo and aqueous phase. Moreover, the Fe-(N9N10)-like interaction involving 2-MCTH is the strongest, as the interaction with iron obeys the following order: 2-MCTH > 2-MCTH (NH<sup>+</sup>)<sub>2</sub> > 1-MCTH > 1-MCTH(NH<sup>+</sup>)<sub>2</sub> in accordance with electrochemical results.

---

**Keywords:** Acid solution; Iron surface; DFT calculations; Dynamic Monte Carlo calculations; Corrosion inhibitive performance.

## 1. INTRODUCTION

Acid solutions are widely used in industry for the elimination of localized deposits due to their aggressiveness. However, it causes a partial dissolution on metal surface, hence there is a need to add the corrosion inhibitors which act by chemical or physical adsorption to limit its attack [1-3]. The choice of inhibitor depends on its efficiency at low concentration as well as medium, but especially the kind of exposed metal surface. Corrosion inhibition in acid medium can be highlighted by the study of adsorption isotherms and multi-spectroscopic investigation of the metal surface [4-6]. Moreover, the structure of the inhibitor play a main role in the interactions mechanism with the metal surface [3, 7].

Inhibitors in an acid medium require the polar group: O, N or S in compounds, where the molecule can attach to the metal surface [8]. Therefore, thiadiazoles are reputed compounds for their [9] corrosion inhibiting ability together with their other inhibiting properties: antifungal, antibacterial, or enzyme [10].

In this respect, the series of macrocyclic polyether compounds (n-MCTH, n: 1-5), which differ by the number of oxygen atoms of the polyether part of the macrocycle as schematized in Figure 1, has been found as an excellent corrosion inhibitors, even at low concentration ( $10^{-5}$ M). Indeed, a systematic experimental investigation carried out by Bentiss et al with weight loss method (WLM), electrochemical impedance spectroscopy (EIS) and potentiodynamic polarization of these compounds as inhibitors of corrosion of mild steel exposed to 1 M HCl solution or C38 carbon steel exposed to 0.5 M  $H_2SO_4$  solution have shown their very high inhibition efficiency values even at low concentration. For instance, when the concentration in HCl solution is  $10^{-4}$  M, the inhibition efficiency of 1-MCTH and 2-MCTH are 97.7 and 99.0 % respectively with WLM and 98.6 and 98.9 with EIS. Moreover, the inhibition efficiency increases with inhibitors concentration in the order of 5-MCTH > 4-MCTH > 3-MCTH > 2-MCTH > 1-MCTH reaching the maximum value of 99.5% for 5-MCTH at  $10^{-4}$  M in HCl solution and 99.3% for 5-MCTH at  $10^{-4}$  M in  $H_2SO_4$  solution, giving the HCl solution a slight priority in terms of efficiency. In the same context, the nature of the interaction between these compounds with the steel interface testing different adsorption isotherms was studied, it is founded that all these compounds obeys a Langmuir adsorption isotherm on the carbon steel surface, which is more related to chemisorption process while the crystallographic investigation has shown the quasi-planarity of 3-MCTH [10-12].

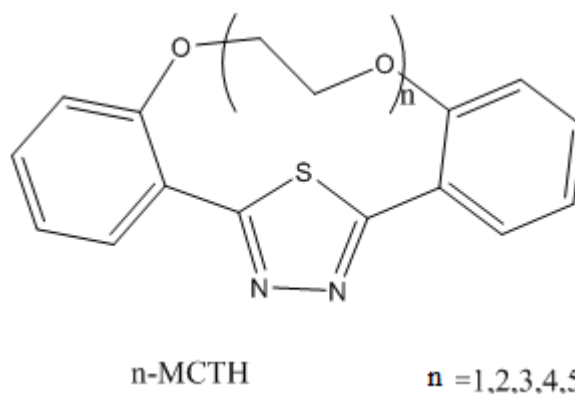


**Figure 1.** 2D structures of the series of macrocyclic polyether compounds (n-MCTH, n: 1-5).

The same authors tried to elucidate the mechanism of n-MCTH inhibition of corrosion as well as the intrinsic reasons for their inhibition efficiency classification via quantum modeling based on B3LYP/6-31G(d,p) DFT method. However, the prediction of a limited number of global descriptors ( $E_{\text{HOMO}}$ ,  $E_{\text{LUMO}}$ ,  $\Delta E$ ,  $\mu$ , molecular area and CCCS dihedral angle) remains very deficient towards a deep understanding of the anti-corrosive adsorption. That's why, we have largely explored the ab initio and molecular dynamics interaction of iron surface with n-MCTH to elucidate the impact of thiadiazole nucleus enriched by the aromatic rings electrons and especially that of the oxygen atoms of the polyether part of the macrocycle. In order to achieve this, we have explored a set of intrinsic processes related the adsorption phenomenon:

- the partial planarity of the molecular structure and surface coverage of the adsorption,
- the electronic transfer between molecular orbitals within the inhibitor and the possibilities of weakening a bonding molecular orbital in favor of an anti-bonding one
- the local reactivity, the polarizability and the competition between local active sites as the inhibitors contains O, N and S atoms,
- the competition between neutral and protonated forms of each inhibitor in acidic medium,
- the complexation modes between inhibitor and metal and their binding strength according to the quantum aspect as well as the dynamic one,
- Solvent effect

In the present communication, we present ab initio and molecular dynamics investigations of iron surface interactions with two macrocyclic polyether compounds 1-MCTH and 2-MCTH, reported in Figure 2, in vacuo and in aqueous solution, before extrapolating the study to the remaining molecules of the series n-MCTH ( $n = 3-5$ ) [13].

## 2. COMPUTATIONAL CONSIDERATIONS

### 2.1. Molecular quantum descriptors

The n-MCTH potential of inhibition was related to their molecular structures and electronic chemical reactivity. Before evaluating the chemical adsorption of these compounds, the B3LYP/6-31G\*\* optimized structures of their neutral and protonated states [14] were carried out, some crucial quantum descriptors of electronic reactivity [15,16] were also evaluated such as  $E_{\text{HOMO}}$  the energy of highest occupied molecular orbital,  $E_{\text{LUMO}}$  the energy of the lowest unoccupied molecular orbital and the energy gap  $\Delta E$ .

$$\Delta E = E_{\text{LUMO}} - E_{\text{HOMO}} \quad (1)$$

Increasing values of  $E_{\text{HOMO}}$  facilitates the electron donating ability of the molecule while increasing  $E_{\text{LUMO}}$  ones facilitates its electron accepting ability. Consequently, it was obviously found a suitable correlation between the rate of corrosion and  $\Delta E$ , lower values of the energy gap  $\Delta E$  provide higher reactivity of the inhibitor [17]. According to Koopmans theorem [18],  $E_{\text{HOMO}}$  and  $E_{\text{LUMO}}$  of the

inhibitor are related to the ionization potential ( $I = -E_{\text{HOMO}}$ ) and the electron affinity ( $A = -E_{\text{LUMO}}$ ). Then, absolute electronegativity ( $\chi$ ) and hardness ( $\eta$ ) of the inhibitor are approximated as follows:

$$\chi = \frac{I+A}{2} \quad (2)$$

$$\eta = \frac{I-A}{2} = \frac{\Delta E}{2} \quad (3)$$

The chemical hardness reflects the resistance towards the deformation or the polarization of the inhibitor electron cloud under small perturbations of chemical reaction. Unlike hardness ( $\eta$ ), softness ( $S$ ) is a global chemical descriptor measuring the molecular reactivity. So, a more reactive inhibitor (small energy gap) is necessarily soft [19].

$$S = \frac{1}{\eta} \quad (4)$$

The fraction of electrons  $\Delta N$  transferred from inhibitor to metal surface, is given by [20,21].

$$\Delta N = \frac{\chi_{\text{Fe}} - \chi_{\text{inh}}}{2(\eta_{\text{Fe}} + \eta_{\text{inh}})} \quad (5)$$

Where  $\chi_{\text{Fe}}$  and  $\chi_{\text{inh}}$  are the absolute electronegativity of iron and inhibitor, respectively, while  $\eta_{\text{Fe}}$  and  $\eta_{\text{inh}}$  denote their absolute hardness, respectively. In order to calculate  $\Delta N$ , a theoretical value of  $\chi_{\text{Fe}} = 7.0$  eV and  $\eta_{\text{Fe}} = 0.0$  were adopted, assuming that for a metallic bulk,  $I$  is equal to  $A$  [22].

The global electrophilicity index  $\omega$  were measured the propensity of the inhibitor to accept electrons. In other words, it's defined as the energy lowering due to the maximal electron flow between inhibitor and metal. Then, a good nucleophile is characterized by lower value of  $\omega$ , and *vice versa* [23].

$$\omega = \frac{\chi^2}{2\eta} \quad (6)$$

## 2.2. Local reactivity using Fukui Functions

To analyze the behavior of different sites in the inhibitor, it is necessary to assess the local reactivity using Fukui functions. These are defined as the first derivative of the electron density  $\rho(\mathbf{r})$  with respect to the number of electrons  $N$  in a constant external potential  $V(\mathbf{r})$  produced by the nuclei or as the functional derivative of the chemical potential  $\mu$  respect to the potential  $V(\mathbf{r})$  at a constant electron number. That's why the Fukui indexes were calculated at the same equilibrium geometry as the original molecule, when adding or removing an electron. Then, the information on the polarization of the electron density upon the change in number of electrons was preserved [24].

$$fk = \left( \frac{\partial \rho(\mathbf{r})}{\partial N} \right) v(\mathbf{r}) = \left( \frac{\partial \mu}{\partial v} \right) N \quad (7)$$

For an electron-transfer controlled reaction, Fukui functions informed about the sites in a molecule on which nucleophilic, electrophilic or radical attacks are most probable [25]. The condensed Fukui functions were calculated, here, by applying finite difference approximation [26], giving the following deductions:

$$fk+ = qk(N + 1) - qk(N) \quad (8)$$

$$fk- = qk(N) - qk(N - 1) \quad (9)$$

$$fk0 = [qk(N + 1) - qk(N)]/2 \quad (10)$$

where  $qk(N + 1)$ ,  $qk(N)$  and  $qk(N - 1)$  represent the net charge of the atom  $k$  in the inhibitor at  $(N + 1)$ ,  $N$  and  $(N - 1)$  electrons, respectively;  $f_k^+$ ,  $f_k^-$  and  $fk0$  are the index of the nucleophilic, electrophilic and radical attack, respectively.

### 2.3. Natural bonding orbital calculations

The interactions due to overlap between bonding and antibonding orbitals give rise to intramolecular charge transfer (ICT) causing stabilization of the molecule [27]. These interactions are observed as an increased in electron density of antibonding orbital that weakens the respective bonds. The delocalization energies associated with the ICT were examined using the second order perturbation theory of the Fock matrix in the NBO method [28,29]. For each donor ( $i$ ) and acceptor ( $j$ ), the stabilization energy  $E(2)$  associated with the delocalization  $i/j$  is calculated as:

$$E^2 = \Delta E_{ij} = q_{ij} (F_{ij}^2 / \epsilon_j - \epsilon_i) \quad (11)$$

Where  $q_i$  is the orbital occupancy,  $E_i$  and  $E_j$  are the diagonal elements and  $F(i,j)$  is the off-diagonal NBO Fock matrix element [30].

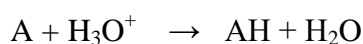
### 2.4. Proton Affinity

Generally, the protonated species have been reported as to take a part in adsorption on the metal surface. As the preferred site for protonation corresponds to the lowest proton affinity PA, the comparison of its values, at different sites, is clearly primordial [31-33]. PA is evaluated as

$$PA = E_{prot} + E_{H_2O} - (E_{neutral} + E_{H_3O^+}) \quad (12)$$

Where  $E_{prot}$  and  $E_{neutral}$  are the total energies of the protonated and the non-protonated inhibitors respectively,  $E_{H_2O}$  is the water molecule total energy and  $E_{H_3O^+}$  is the hydronium ion total energy.

Since the protonation follows the reaction below:



### 2.5. Molecular quantum and dynamic optimizations

All geometry optimizations and quantum chemical calculations were performed using the density functional theory using method B3LYP (the Becke's three Parameter Hybrid Functional using the Lee–Yang–Parr correlation functional) [34] at 6-31G (d,p) basis set, by means of the Gaussian 2009 program package [35]. To model the solvation effect, the PCM (Polarizable Continuum Model) considering the solvent as a continuum and the solute in its cavities, was adopted [36].

Molecular dynamic simulation was carried out with the Metropolis Monte Carlo methodology [37-39] using the adsorption locator and Forcite codes implemented in the Material Studio 7.0 software [40]. The Monte Carlo simulation allows to locate the most stable configuration of the interaction between inhibitor molecules and iron surface, i.e. the stronger adsorption region corresponds to the higher negative adsorption energy. The ab initio force field named COMPASS II (Condensed phase Optimized Molecular Potentials for Atomistic Simulation Studies) [33] was used to optimize the structures of all components of the inhibitor-iron surface system in the dynamic Monte Carlo study. The simulation was carried out with Fe (111) crystal surface in a simulation box (17.89×17.89×38.34Å) with periodic boundary conditions in order to simulate a representative part of an interface. The Fe (111) plane was next enlarged to a (9×9) super cell. After that, a vacuum slab with 3.0 nm thickness was built above the Fe (111) plane. To mimic the real experimental corrosion environment, 50 molecules of water was added to the simulation box. Although Fe (110) plane is a densely-packed surface, the crystallographic surface Fe (111) was chosen because of the lower value of its formation energy [41], knowing that the surface energy is evaluated based on the Gibbs relation [42]:

$$E_{\text{surf}} = (E_{\text{slab}} - E_{\text{bulk}}) / 2A \quad (13)$$

Where  $E_{\text{surf}}$  is the energy of the system with surface,  $E_{\text{bulk}}$  is the energy of the bulk system having the same number of atoms and  $A$  is the surface area of the computing cell.

Regarding the experimental inhibition efficiency compared with all these theoretical parameters, even there is a good agreement between the percentage values of inhibitory efficiencies  $E_{\text{WL}}$ ,  $E_{\text{EIS}}$  and  $E_{\text{PP}}$  determined respectively by gravimetry (WL), electrochemical impedance spectroscopy (EIS) and potentiodynamic polarization (PP), it is matter to differentiate between them [43]. Indeed, the corrosion rate (CR) and inhibition efficiency  $E_{\text{WL}}$  for the gravimetric method are calculated as follows:

$$\text{CR} = 87.6(wa - wp) / \rho A t \quad (14)$$

and

$$E_{\text{WL}} \% = 100 (wa - wp) / wa \quad (15)$$

Where  $wa$  and  $wp$  are respectively weight loss in absence and presence of inhibitors,  $\rho$  is the density of iron,  $A$  is the area of the mild steel strip and  $t$  is the immersion time. For electrochemical methods, inhibition efficiency is calculated as follows:

$$E_{\text{EIS}} \% = [1 - Ra/Rp] \times 100 \quad (16)$$

Where,  $R$  is the sum of  $R_{ct}$  (charge transfer resistance) and  $R_f$  (film resistance),  $R_a$  and  $R_p$  are the polarization resistance in absence and presence of inhibitors respectively

$$E_{PP} \% = [1 - I_p / I_a] \times 100 \quad (17)$$

Where  $I_a$  and  $I_p$  are the uninhibited and inhibited corrosion current densities, respectively.

### 3. RESULTS AND DISCUSSION

#### 3.1. Regioselectivity of isolated neutral species and in aqueous solution

The regioselectivity, which plays a key role in the chemical reactivity, is highly dependent on steric and electronic factors. For this reason, the structural and electronic properties of 1-MCTH and 2-MCTH were analyzed, the results have shown that they have a strong effect on the efficiency of corrosion inhibition. The optimized geometries of 1-MCTH and 2-MCTH, with their respective symmetry  $C_1$  and  $C_s$  are shown in Figure 2.

##### 3.1.1. Selected geometrical parameters

The consultation of some crucial structural parameters, reported in Table 1, shows that the addition of CCO functional group in 2-MCTH, compared with 1-MCTH, makes the ring containing oxygens less constrained (for example C24O26 and C25O27 increase of about  $0.06 \text{ \AA}$ ). Consequently, the distance between two aryls increases (C24C25 distance increases of about  $1.16 \text{ \AA}$ ) and their interaction decreases allowing them to be in the same plane, as the dihedral angle C20-C3-C11-C22 increases from  $-15^\circ$  to  $0^\circ$  (or C16-C24-C25-C18 decreases from  $15$  to  $0^\circ$ ).

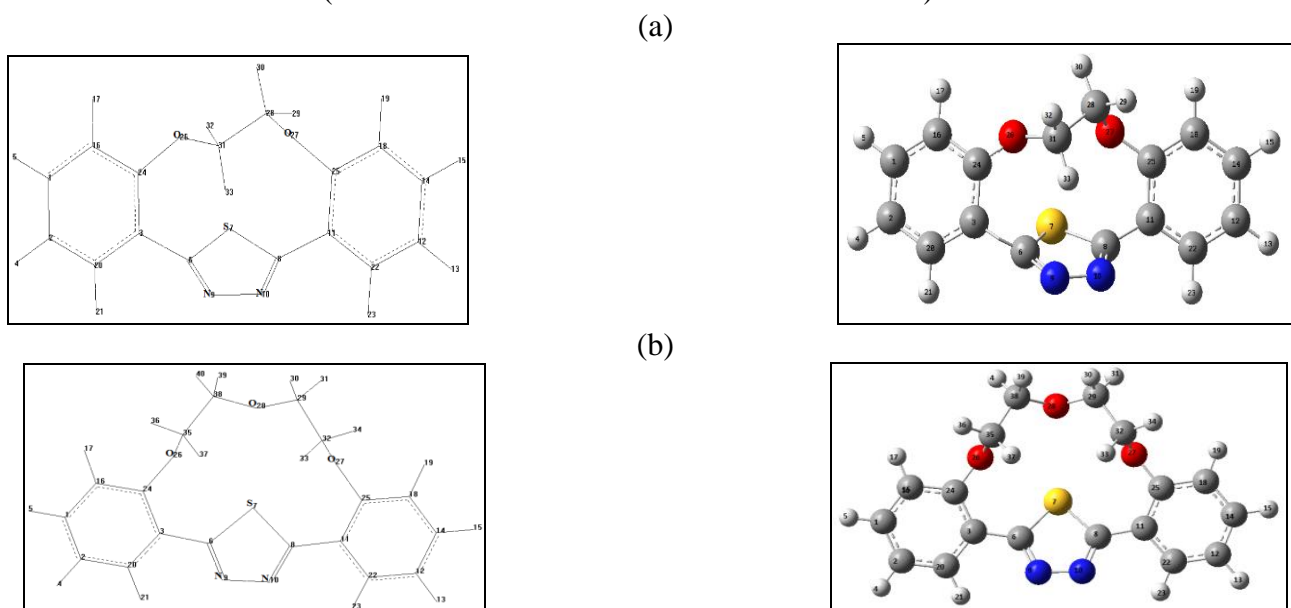


**Figure 2.** Structures (2D) and optimized structures schematic representation of 1-MCTH (a) and 2-MCTH (b) at B3LYP/6-31G\*\*.

Moreover, the dihedral angle (C24-C3-C6-S7) locating the thiadiazole ring, is lower for 2-MCTH ( $-15^\circ$ ) by about  $38^\circ$  than in 1-MCTH ( $-53^\circ$ ), like the dihedral angle C25C11C8S7 which decreases from  $48^\circ$  to  $15^\circ$ , implying that 2MCTH is close to the planar structure, compared to 1-MCTH.

We further noted that the dihedral angle O26C3C11O27 was also reduced of about  $16^\circ$ . However, the increasing of the planarity degree of 2-MCTH makes the aryl segments closer to the thiadiazole ring, with a decrease of C3-C6 of about  $0.07 \text{ \AA}$  and C8-C11 of about  $0.05 \text{ \AA}$ , N9N10 decreases also of about  $0.22 \text{ \AA}$ . Thus, the comparative analysis of the two optimized structures showed that 2-MCTH is more planar and its ring segments are closer, indicating the tendency of the set of the molecules n-MCTH (n=1-5) towards planarity as the oxygen number of the macrocyclic polyether part increases. Indeed, X-ray crystallographic analysis of 4-MCTH, of which the macrocyclic polyether entity contains 5 oxygen atoms, has shown that the structure belongs to the C 2/c space group of the monoclinic system and is practically plane. The phenyl rings planes are shifted relative to the thiadiazole ring plane by an angle only equal to  $4.93$ . In addition, a weak hydrogen bond connects the polyether macrocyclic oxygens and phenyls, providing two-dimensional stability of the crystalline system [10].

Concerning the solvent effect, it's more noticeable for 2-MCTH as the dihedral angle (C24-C3-C6-S7 or C25-C11-C8-S7), is reduced of about  $3^\circ$ , making this molecule in aqueous solution relatively more planar.

**Table 1.** Bond distance ( $\text{\AA}$ ) and Torsional angle ( $^\circ$ ) for the neutral inhibitors 1-MCTH and 2-MCTH optimized structures and their double protonated (N9H+N10H+) and (O26H+O27H+) optimized forms, in vacuo (G) and in aqueous solution (A) at B3LYP/6-31G\*\*

Bonds distances ( $\text{\AA}$ )	1MCTH (G)	1MCTH (A)	1MCTHN <sub>9</sub> H+ N <sub>10</sub> H+ (G)	1MCTHN <sub>9</sub> H+ N <sub>10</sub> H+ (A)	1MCTHO <sub>26</sub> H+O <sub>27</sub> H+ (G)	1MCTHO <sub>26</sub> H+O <sub>27</sub> H+ (A)
C3-C6	1.475	1.474	1.434	1.445	1.478	1.476
C6-S7	1.742	1.739	1.730	1.723	1.764	1.747
C8-S7	1.742	1.735	1.735	1.728	1.773	1.749
C6-N9	1.314	1.317	1.340	1.329	1.300	1.311
C8-N10	1.315	1.318	1.348	1.335	1.302	1.311
C8-C11	1.473	1.469	1.426	1.439	1.473	1.473
C24-O26	1.384	1.384	1.376	1.378	1.506	1.475
C25-O27	1.380	1.381	1.356	1.361	1.510	1.475
N9-N10	1.364	1.366	1.377	1.360	1.367	1.366
S7-O26	2.987	2.966	2.607	2.666	2.971	3.094
S7-O27	2.874	2.863	2.530	2.577	3.143	2.985
N9-O26	3.691	3.684	3.963	3.900	3.517	3.663
N10-O27	3.779	3.801	3.967	3.909	3.736	3.764
C24-C25	5.222	5.229	5.099	5.120	5.436	5.480
C3-C11	5.070	5.071	5.018	5.047	5.132	5.117
Bonds distances ( $\text{\AA}$ )	2MCTH (G)	2MCTH (A)	2MCTHN <sub>9</sub> H+ N <sub>10</sub> H+ (G)	2MCTHN <sub>9</sub> H+ N <sub>10</sub> H+ (A)	2MCTHO <sub>26</sub> H+O <sub>27</sub> H+ (G)	2MCTHO <sub>26</sub> H+O <sub>27</sub> H+ (A)
C3-C6	1.468	1.467	1.423	1.432	1.471	1.437



O26-C3- C11-O27	0.000	0.000	0.000	0.000	0.000	-0.086
C24-O26- O27-C25	0.000	0.000	0.000	0.000	0.000	-0.185
O26-C35- C32-O27	0.000	0.000	0.000	0.000	0.000	-0.353
C28-N9- N10-C31	0.000	0.000	0.000	0.000	0.000	-0.186

### 3.1.2. Quantum chemical parameters

Beside the differentiation between 1-MCTH and 2-MCTH geometries, an analysis of HOMO, LUMO and related quantum parameters also provided valuable information on their selectivity and reactivity. Further, it's well known that HOMO indicates the regions of the molecule that have a tendency to donate electrons to electrophilic species while the LUMO predicts the regions of the molecule with high tendency to accept electrons from nucleophilic species. The shape and symmetry of HOMO and LUMO are also important in predicting the reactivity [44]. The results presented in Figure 3 show that for 1-MCTH, HOMO is delocalized throughout the molecule, except for sulfur atom S of thiadiazole and C16, C18, C20 and C22 of aryl rings which are excluded from the electron donation regions, while LUMO is strongly localized on thiadiazole ring, with a very significant electron acceptor effect for S. For 2-MCTH, HOMO as well as LUMO are spread out on all the atoms (except C2, C12, C16, C18) of aryl rings fused to the thiadiazole ring (except S for HOMO). It must be concluded that the thiadiazole ring is a very important region for donating or accepting electrons. Moreover, while it is easy to verify that all oxygen atoms can't receive electrons, we noticed that the central oxygen for 2MCTH can't donate electrons.

Neutral inhibitors	HOMO	LUMO	T.D. HOMO	T.D.LUMO
1-MCTH				
2-MCTH				

**Figure 3.** HOMO, LUMO and total density charge (T.D) of the B3LYP/6-31G\*\* optimized neutral inhibitors 1-MCTH and 2-MCTH in vacuo.

Overcoming the deficiency of the simplistic theoretical part of the work on n-MCTH by Bentiss et al [10,12] who were satisfied only with the comparison of the values of HOMO, LUMO energies, and for the purpose of a complete quantification of the reactivity of the two molecules 1-

MCTH and 2-MCTH, Table 2 shows the set of quantum chemical parameters values. In this context, the molecule, with lower absolute values of the energy gap  $\Delta E$ , exhibits higher inhibition efficiencies. While  $E_{LUMO}$  remains practically constant,  $E_{HOMO}$  substantially increases from 1-MCTH to 2-MCTH, leading to decreases of  $\Delta E$  indicating that the ability to donate electrons to metal surface is better for 2-MCTH than 1-MCTH. These are also expressed by the values of global softness, and further confirmed by the fraction of electrons ( $\Delta N$ ) transferred from the inhibitor to iron. The metals would preferentially interact with inhibitors that have high  $S$  and low  $\eta$  values, as the soft inhibitor with the lower value of  $\Delta E (= 2\eta)$ , exchange easily electrons with their environment.

According to different authors [45,46], when the value of  $\Delta N$  is positive and lower than 3.6 eV, it suggests that the inhibitor have strong tendency to donate electrons to the vacant d-orbital of metal, as  $\Delta N$  value is the net electron transferred from the inhibitor molecules to the metal surface. From the Table 2, the value of  $\Delta N$  in case of 2-MCTH (0.701eV) is greater than 1-MCTH (0.583eV) one, confirming that the two molecules can donate electrons to the vacant d-orbital of iron surface favouring the formation of adsorptive bonds, with a slight superiority for the former, which is confirmed by its lower electronegativity. The decrease in the value of electronegativity leads to a decrease of the global electrophilicity index, and therefore an increase of the nucleophilic character of 2MCTH, as the good nucleophile is characterized by lower value of  $\omega$ . Moreover, it's also reported that an increase in the inhibition efficiency can also be related to the increase in the dipole moment which informs about the polarity of the molecule [47]. As can be seen from Table 2, 2-MCTH has a significantly larger dipole moment.

**Table 2 .** Some quantum chemical parameters for the B3LYP/6-31G\*\* optimized neutral inhibitors 1-MCTH and 2-MCTH, in vacuo (G) and in aqueous solution (A)

	Phase	$E_{HOMO}$	$E_{LUMO}$	$\Delta E$	$\Delta N$	$X$	$\Omega$	$S$	$\mu$	$E_{EIS}$	$E_{WL}$
1-MCTH	G	-6.600	-1.800	4.800	0.583	4.200	3.675	0.417	2.600	98.6	97.7
	A	-6.480	-1.780	4.700	0.611	4.130	3.629	0.426	3.800		
2-MCTH	G	-6.130	-1.810	4.320	0.701	3.970	3.648	0.463	5.070	98.9	99.0
	A	-6.150	-1.790	4.360	0.695	3.970	3.615	0.459	7.600		

All energy values are in eV;  $\mu$ : the dipole moment in Debye;  $S$ : the global softness in  $\text{eV}^{-1}$ ;  $E_{EIS}$   $E_{WL}$  are the average experimental percent inhibition efficiency (%), obtained respectively from electrochemical impedance spectroscopy and weight loss method as given in [8,9].

Inspection of solvation results shows that only slight difference in HOMO energy of 1-MCTH can be observed leading to an increase of  $\Delta E$  of about 0.1eV, influencing slightly the other electronic parameters such as the softness which increases of about  $0.01\text{eV}^{-1}$ . The electron transfer fraction and the global nucleophilicity have increased of 0.03 and 0.04, respectively. The electronic change of 1-MCTH has not changed the order of the electron donating abilities of these molecules. Even no significant change was observed for 2-MCTH under the solvent effect, except the obvious increase in the dipole moment, the electron donating ability order of these molecules remains unchanged.

Combining with the results of frontier orbital energies of isolated molecules and in aqueous solution, we can conclude that 2-MCTH is more reactive in both gas and aqueous phase.

### 3.2. Local reactivity and population analyses of isolated neutral species and in aqueous solution

#### 3.2.1. Local reactivity based on FUKUI indices

Fukui indices provide information about which atoms in a molecule have a larger tendency to accept an electron from the metal surface, these atoms thus more prone to undergo a nucleophilic attack ( $f_{k+}$  highest absolute value), the atoms with tendency to donate electron to the metal surface are more prone to undergo an electrophilic attack ( $f_{k-}$  highest absolute value) [48,49]. It is well documented that Nitrogen (N) and Sulfur (S) constitute a good adsorption centers, due to their high polarizability and lower electronegativity, and compounds having these heteroatoms behaved as good inhibitors. It is also worth noting that organic inhibitors having nitrogen are better inhibitors in aggressive hydrochloric acid whereas organic inhibitors having sulfur are better in sulphuric acid. Compounds possessing sulfur and nitrogen like n-MCTH are an excellent corrosion inhibitors for both media [50-52].

A computational condensed Fukui functions of some thiophene derivatives carried out by L.Guo et al [53] reveals that, in agreement with HOMO and LUMO orbital densities, nitrogen atoms constitute a nucleophilic sites, donating electrons to vacant molecular orbital on the iron surface to form coordinate bond while sulphur atom of the thiophene ring constitutes an electrophilic attack site through which the molecule accepts electrons to form feedback bonds with iron surface.

The calculated condensed Fukui functions for the non-hydrogen atoms of the two molecules 1-MCTH and 2-MCTH are presented in Table 3. It can be seen for 1-MCTH that S, C8, N9 and N10 in the thiadiazole ring are the most susceptible sites for the nucleophilic attacks as they present the highest values of  $f_{k+}$ , 0.176 for S, 0.132 for C8, 0.051 and 0.043 for N9 and N10, respectively, without ignoring the  $f_{k+}$  values 0.041 for C12 and 0.037 for C24 of aryl rings. On the other hand, S, N10, N9 and C6 are the most susceptible sites for the electrophilic attacks as they present the highest values of  $f_{k-}$ , 0.078 for S, 0.068 for N10, 0.054 for N9 and 0.063 for C6. It can be concluded for 1-MCTH that the thiadiazole ring is the most active region responsible of both donating and accepting electrons towards adsorption on iron surface. It's worthwhile noticing that N10 is slightly more susceptible to donate electron than N9, and vice versa. In the same context, C6 which is directly bonded to N9, is susceptible to donate electron while C8, which is directly bonded to N10, is susceptible to accept electron. This is most likely due to the impact of asymmetric oxygen environment in the molecule (Figure. 2). In addition to the reactivity of the thiadiazole ring like for 1MCTH, the two aryl rings contribute to the total reactivity of 2MCTH, by electron donating or accepting of C1, C3, C11 and C14, which exhibit  $f_{k+}$  and  $f_{k-}$  values around 0.05, and for C20, C22, C24 and C25 with  $f_{k+}$  and  $f_{k-}$  values of about 0.03, suggesting that 2MCTH is more efficient in terms of inhibition compared to 1MCTH. For both molecules, the oxygen atoms have a relatively low  $f_{k-}$  and  $f_{k+}$  indices values in contrast to  $f_{k_0}$  there by demonstrating their susceptibility to essentially undergo free radical attacks.

The sulfur atom is more susceptible to receive electron than to donate it to the metal surface. We further noted with interest that water as solvent has no significant effect on the local reactivity,

based on Fukui index. Fortunately, the local reactivity results corroborate those obtained by molecular quantum parameters.

**Table 3.** The condensed Fukui functions on the atoms of the B3LYP/6-31G\*\* optimized neutral inhibitors 1-MCTH and 2-MCTH. *in vacuo* (G) and *in aqueous solution* (A).

1-MCTH (G)		1-MCTH (A)		2-MCTH (G)		2-MCTH (A)			
Atoms	fk+	fk-	fk+	fk-	Atoms	fk+	fk-	fk+	fk-
1 C	0.023	0.025	0.016	0.031	1 C	0.047	0.049	0.045	0.046
2 C	0.025	0.003	0.018	0.004	2 C	0.018	0.010	0.017	0.009
3 C	0.027	-0.015	0.027	-0.015	3 C	0.049	0.047	0.048	0.046
6 C	0.001	0.063	0.002	0.061	6 C	0.040	0.035	0.040	0.038
7 S	0.176	0.078	0.177	0.075	7 S	0.142	0.096	0.138	0.090
8 C	0.132	0.030	0.128	0.034	8 C	0.046	0.035	0.040	0.038
9 N	0.051	0.054	0.051	0.054	9 N	0.040	0.053	0.039	0.052
10 N	0.043	0.068	0.043	0.067	10 N	0.040	0.053	0.039	0.052
11 C	0.007	0.004	0.008	0.005	11 C	0.049	0.047	0.048	0.046
12 C	0.041	-0.017	0.041	-0.017	12 C	0.018	0.010	0.017	0.009
14 C	0.021	0.031	0.020	0.031	14 C	0.047	0.049	0.045	0.046
16 C	0.005	0.002	0.007	0.002	16 C	0.018	0.013	0.018	0.013
18 C	0.019	0.002	0.018	0.003	18 C	0.018	0.013	0.018	0.013
20 C	0.012	0.02	0.011	0.022	20 C	0.035	0.028	0.033	0.025
22 C	0.015	0.019	0.017	0.021	22 C	0.035	0.028	0.033	0.025
24 C	0.037	0.002	0.038	0.002	24 C	0.031	0.029	0.031	0.029
25 C	0.015	0.03	0.013	0.029	25 C	0.031	0.029	0.031	0.029
26 O	0.027	0.013	0.026	0.014	26 O	0.001	0.010	0.001	0.010
27 O	0.031	0.012	0.031	0.013	27 O	0.001	0.010	0.001	0.010
28 C	-0.006	-0.023	-0.009	-0.021	28 O	0.009	0.013	0.009	0.013
31 C	0.017	-0.003	0.019	-0.004	29 C	-0.002	-0.002	-0.002	-0.002
-	-	-	-	-	32 C	-0.023	-0.027	-0.025	-0.028
-	-	-	-	-	35 C	-0.023	-0.027	-0.025	-0.028
-	-	-	-	-	38 C	-0.002	-0.002	-0.002	-0.002

### 3.2.2. Natural population atomic charges and natural bond orbital analyses

The partial atomic charge on the atoms is also a local molecular parameter which indicates the atomic regions of the molecule on which certain types of reactions are likely to occur. The interaction between the metal and the inhibitor is often considered to preferentially take place on the atom with the highest negative charge. The molecular charge distribution in terms of NPA charges are reported in Figure. 3. The highest negative charge was located only on oxygen and nitrogen heteroatoms excluding sulfur, which suggests that these centers have highest electron density and would preferentially interact with the metal surface. Oxygen was given first priority, however, the axial orientation of nitrogen lone pair electrons may give it the advantage compared to oxygen where the lone pairs are oriented equatorially. It should also be noted that the partial atomic charges of 2-MCTH nitrogen's are more negative than 1-MCTH.

Concerning the NBO analyses, the E(2) stabilization energy indicates the direct relationship between the intensity of ICT and the interaction bonding - antibonding orbitals. These interactions are observed as an increase in electron density of anti-bonding orbital that weakens the respective bonds [54]. Table 4 showed that the strongest intramolecular charge transfer is from  $\pi$  C-C to  $\pi^*$  C-C within the same phenyl radical with stabilization energy of about 20 kcal/mol, in 1-MCTH as well as 2-MCTH. However, there occurs a strong intramolecular charge transfer only in 2-MCTH, from  $\pi$  C3-C24 to  $\pi^*$  C6-N9 and  $\pi$  C11-C25 to  $\pi^*$  C8-N10, weakening  $\pi$  C6-N9 and  $\pi^*$  C8-N10 and leading to stabilization energy of about 16 kcal/mol.

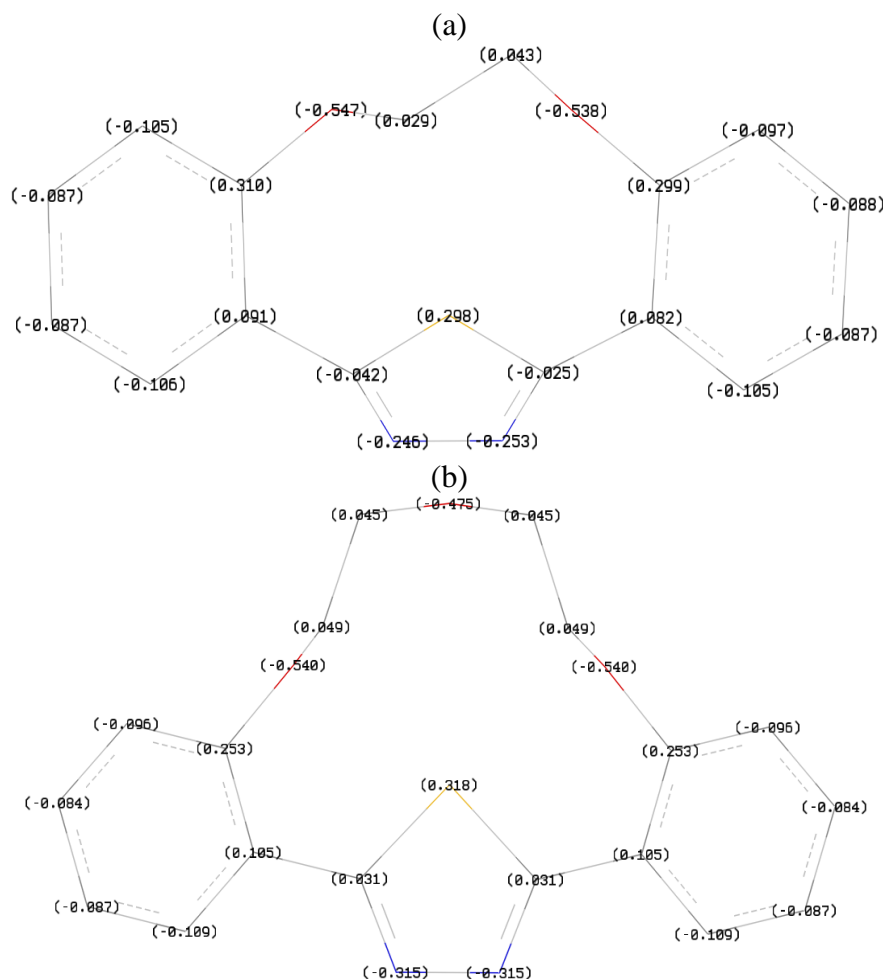


**Figure 4.** NBO charges of the B3LYP/6-31G\*\* optimized neutral inhibitors 1-MCTH (a) and 2-MCTH (b) *in vacuo*.

Moreover, the two molecules are also stabilized by  $\pi$  C6-N9 -  $\pi^*$  C8-N10 and  $\pi$  C8-N10 -  $\pi^*$  C6-N9 interactions, that weakens  $\pi$  C6-N9 and  $\pi$  C8-N10 once again, leading to stabilization energy of about 13 kcal/mol for 1-MCTH and 10 kcal/mol for 2-MCTH. Consequently, the low electronic density of C-N strengthens that of nitrogens which become more aggressive for 2-MCTH compared to 1-MCTH.

## 3.2.3. Population analyses based on the Molecular Electrostatic Potential

The molecular electrostatic potential (MEP) is useful to predict the reactive behavior of the molecule [5]. The MEP surface is on overlaying of the electrostatic potential on to the isoelectronic density surface. This is a valuable tool for describing overall molecule charge distribution as well as anticipating sites of electrophilic addition. While red color (low electrostatic potential energy value) represents high negative charges, blue color (high electrostatic potential energy value) represents strongly positive region. The predominant green region in the MEP surfaces corresponds to a potential halfway between the two extremes red and blue region, knowing that yellow color is very close to red color in terms of electrostatic potential energy intensity.

**Table 4.** Second Order Perturbation theory analysis of Fock matrix in NBO basis for 1-MCTH and 2-MCTH by B3LYP/6-31G\*\*. (E (2) means energy of hyper conjugative interactions).

Donneurs	Accepteurs	E(2)(kcal/mol) 1-MTCH	E(2)(kcal/mol) 2-MTCH
$\pi$ C1 - C2	$\pi^*$ C 16 - C 24	19,650	
$\pi$ C1 - C16	$\pi^*$ C 2 - C 20	-	18,280
	$\pi^*$ C 3 - C 24	-	20,860
	$\pi^*$ C 1 - C 16	-	21,640
	$\pi^*$ C 3 - C 24	-	20,350
$\pi$ C3 - C20	$\pi^*$ C 1 - C 2	18,400	-
	$\pi^*$ C 16 - C 24	20,970	-
	$\pi^*$ C 1 - C 16	-	18,460
	$\pi^*$ C 2 - C 20	-	18,940
	$\pi^*$ C 6 - N 9	-	15,920
$\pi$ C6 - N9	$\pi^*$ C 8 - N 10	12,720	9,440
$\pi$ C8 - N10	$\pi^*$ C 6 - N 9	13,110	9,440
$\pi$ C11 - C22	$\pi^*$ C 12 - C 14	18,790	-
	$\pi^*$ C 18 - C 25	21,540	-
	$\pi^*$ C 8 - N 10	2,130	15,920
	$\pi^*$ C 12 - C 22	-	18,940
	$\pi^*$ C 14 - C 18	-	18,460
$\pi$ C12 - C14	$\pi^*$ C 11 - C 22	22,270	-
	$\pi^*$ C 18 - C 25	19,760	-
$\pi$ C12 - C22	$\pi^*$ C 11 - C 25	-	20,350
	$\pi^*$ C 14 - C 18	-	21,640
$\pi$ C14 - C18	$\pi^*$ C 11 - C 25	-	20,860
	$\pi^*$ C 12 - C 22	-	18,280
$\pi$ C16 - C24	$\pi^*$ C 1 - C 2	20,970	-
$\pi$ C16 - C24	$\pi^*$ C 3 - C 20	18,280	-
$\pi$ C18 - C25	$\pi^*$ C 11 - C 22	18,170	-
	$\pi^*$ C 12 - C 14	20,900	-

The MEP calculated by boucherit et al for 1,18-diaza-(3,4;15,16;- dibenzo)-19,27-oxydianiline-5,8,11,14-tetra oxa cycloheptacosine-1,17-diene noted L which contains nitrogen atoms and macrocyclic polyether cavity shows that the negative regions are mainly located around

heteroatoms [55]. In the same way, the MEP surface picture of 1-MCTH and 2-MCTH, given in Figure 4, reveals that for both molecules, the region of high negative charges is seen around the nitrogens N9 and N10 which are susceptible to electrophilic attack. However, the MEP surface shows significant distribution of negative charge in the oxygen region of 1-MCTH (with more yellow color), which become relatively important in the region of oxygen atoms for 2-MCTH (with red color more pronounced). Thus, the population analysis based on MEP supports nitrogens more than oxygens for metal interaction.

Combining with all global and local electronic proprieties, it can be concluded that 2-MCTH is more reactive because of the noticeable involvement of aryl rings, in addition to thiadiazole ring, in donating and accepting electron process compared to 1-MCTH. In the same context, the nitrogens are more electron donating in the former than the later and the sulfur is only susceptible to accept electrons.

### 3.3. Regioselectivity of isolated protonated species and in aqueous solution

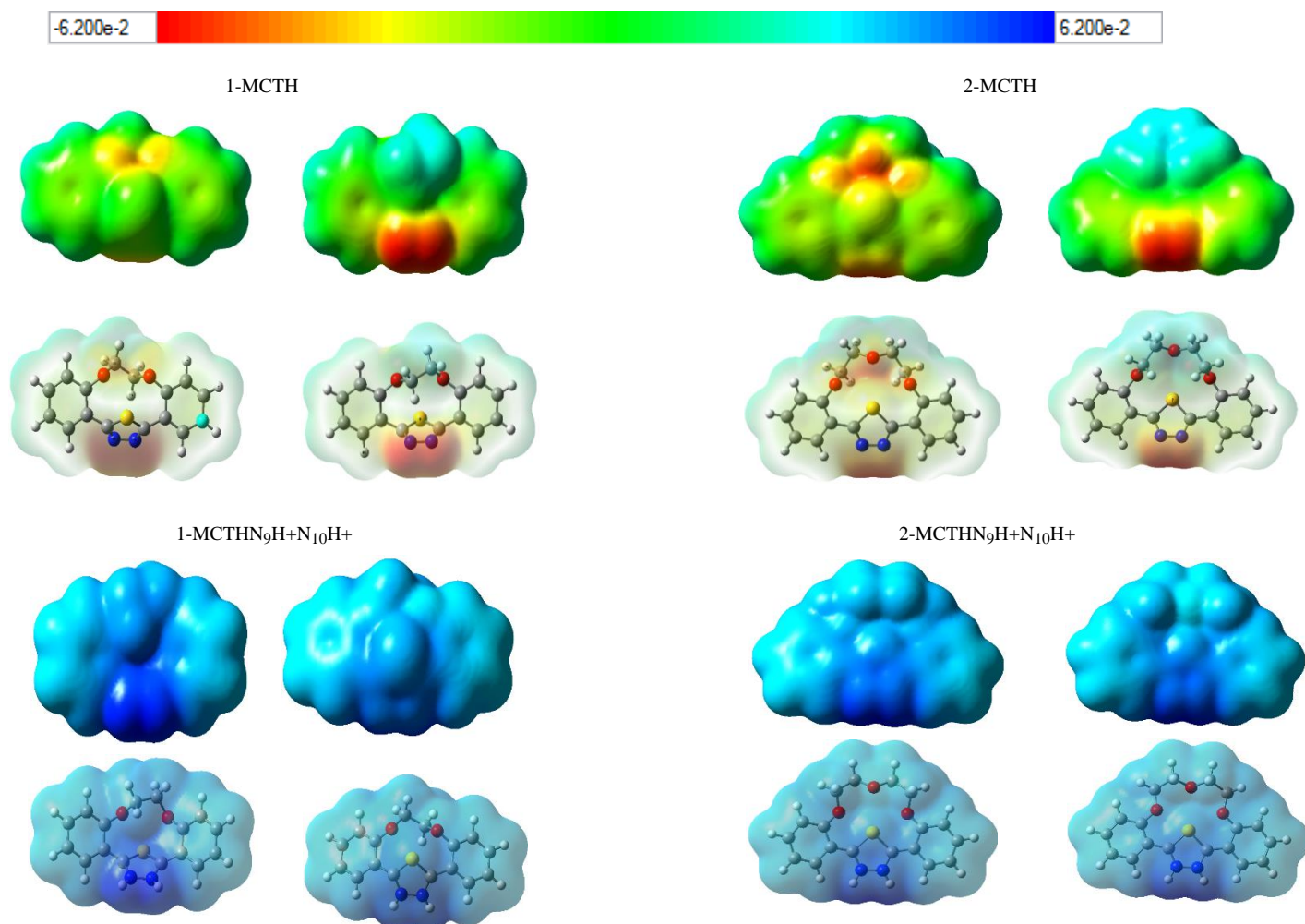


**Figure 5.** Molecular electrostatic potential contour map (MPE) for the neutral inhibitors 1-MCTH and 2-MCTH optimized and their double protonated ( $N_9H+N_{10}H^+$ ) optimized forms. *in vacuo* (G) and *aqueous solution* (A) at B3LYP/6-31G\*\*. (Red: Strong negative electrostatic potential (EP); Yellow: Moderately negative EP; Blue: Strong positive EP; Green: Moderately positive EP).

The process of corrosion inhibition takes place in acidic medium characterized by a high probability of protonation of atoms with lone pair of electrons. Therefore, a competition is possible between the neutral and the protonated form to be adsorbed by the metal surface. For this purpose, it is interesting to investigate the characteristics of the corrosion inhibitor in the protonated forms and to compare them with the non-protonated form. Such a comparison provides information about the preferred form of the inhibitor to interact with the metal surface as the two forms compete to create coordinate bond with iron surface [56,57]. The three atoms on which 1MCTH or 2MCTH could be protonated are N, O and S.

### 3.3.1. Quantum chemical parameters of isolated protonated forms and in aqueous solution

**Table 5.** Some quantum chemical parameters for the B3LYP/6-31G\*\* optimized protonated inhibitors of 1-MCTH and 2-MCTH *in vacuo* (G) and *in aqueous solution* (A).

	Phase	$E_{\text{HOMO}}$	$E_{\text{LUMO}}$	$\Delta E$	$\Delta N$	X	$\Omega$	S	$\mu$	$E_{\text{EIS}}$	$E_{\text{WL}}$
1MCTHN <sub>9</sub> H+N <sub>10</sub> H +	G	-13.400	-10.027	3.373	-	11.714	40.678	0.593	6.700	98.6	97.7
	A	-7.470	-3.700	3.770	0.375	5.585	8.274	0.531	9.810	98.6	97.7
1MCTHN <sub>9</sub> H+	G	-9.900	-6.100	3.800	-	8.000	16.842	0.526	4.100	98.6	97.7
	A	-6.970	-2.970	4.000	0.508	4.970	6.175	0.500	4.770	98.6	97.7
1MCTHN <sub>10</sub> H+	G	-10.100	-5.800	4.300	-	7.950	14.698	0.465	3.140	98.6	97.7
	A	-6.270	-2.610	3.660	0.699	4.440	5.386	0.546	4.310	98.6	97.7
1MCTHO <sub>26</sub> H+O <sub>27</sub> H +	G	-13.700	-9.060	4.640	-	11.380	27.910	0.431	8.490	98.6	97.7
	A	-7.750	-2.820	4.930	0.348	5.285	5.666	0.406	9.730	98.6	97.7
1MCTHO <sub>26</sub> H+	G	-10.150	-5.480	4.670	-	7.815	13.078	0.428	4.670	98.6	97.7
	A	-7.060	-2.240	4.820	0.488	4.650	4.486	0.415	6.480	98.6	97.7
1MCTHO <sub>27</sub> H+	G	-9.980	-5.510	4.470	-	7.745	13.419	0.447	6.060	98.6	97.7
	A	-7.170	-2.510	4.660	0.464	4.840	5.027	0.429	6.070	98.6	97.7
2MCTHN <sub>9</sub> H+N <sub>10</sub> H +	G	-12.800	-9.220	3.580	-	11.010	33.860	0.559	5.510	98.9	99.0
	A	-7.150	-3.400	3.750	0.460	5.275	7.420	0.533	8.390	98.9	99.0
2MCTHN <sub>9</sub> (N <sub>10</sub> )H+	G	-9.170	-5.190	3,98	-	7,18	12,953	0,503	3,060	98,9	99,0
	A	-6.540	-2.690	3.850	0.619	4.615	5.532	0.519	4.140	98.9	99.0
2MCTHO <sub>26</sub> H+O <sub>27</sub> H +	G	-13.067	-8.560	4.507	-	10.814	25.944	0.444	10.180	98.9	99.0
	A	-7.560	-3.750	3.810	0.353	5.655	8.393	0.525	10.590	98.9	99.0
2MCTHO <sub>26</sub> (O <sub>27</sub> )H+	G	-8.990	-4.830	4.160	0.022	6.910	11.478	0.481	9.710	98.9	99.0
	A	-6.980	-2.260	4.720	0.504	4.620	4.522	0.424	14.510	98.9	99.0

All energy values are in eV;  $\mu$ : the dipole moment in Debye; S: the global softness in eV<sup>-1</sup>; EEIS EWL are the average experimental percent inhibition efficiency (%), obtained respectively from electrochemical impedance spectroscopy and weight loss method as given in [8,9].

As evidenced from Table 5, the protonated species has the lower  $E_{\text{HOMO}}$  and  $E_{\text{LUMO}}$  compared to the neutral forms, this suggests that protonation decreases the tendency of the inhibitor to donate electrons and increases its tendency to accept electrons, which is confirmed by the negative  $\Delta N$  values indicating that the electronic exchange is more favorable from the metal to the protonated inhibitor.

Indeed, the protonation reduces the HOMO orbital space at the atom subject to protonation, and thus reduces its capacity to donate electrons. As an illustration, the HOMO and LUMO of 1-MCTHN9H+N10H<sup>+</sup>, 1-MCTHO26H+O27H<sup>+</sup>, 2-MCTHN9H+N10H<sup>+</sup> and 2-MCTHO26H+O27H<sup>+</sup> doubly protonated forms are presented in Figure. 5. With smaller  $\Delta E$  value and thus higher softness, the protonated species (except 2-MCTHO26H+O27H<sup>+</sup>) are more reactive than neutral form. The electrophilicity character also increases as well as the electronegativity. This is the case for instance for 1-MCTHN9H+N10H<sup>+</sup> and 2-MCTHN9H+N10H<sup>+</sup> for which the softness, the electrophilicity index and the absolute value of  $\Delta N$  are the highest among the 1-MCTH and 2-MCTH protonated form quantum parameters values, respectively. On the other hand, the dipole moment is higher for the protonated species than for the neutral species suggesting that dipole interactions are more predominant in the interaction between the metal surface and the protonated form than in the interaction between the metal surface and the neutral form. About the solvent effect on the molecular properties of the protonated species, the reactivity expressed by  $\Delta E$  or  $S$  of the protonated species in aqueous solution is decreased by comparison to its reactivity without solvent. The electrophilicity character also decreases drastically as well as the electronegativity. The dipole moment is higher in aqueous solution compared to the isolated protonated forms, which is a result of the polarization of the protonated inhibitor by the solvent, resulting in an increased charge separation. It should be noted also that  $\Delta N$  values, which are negative for the isolated protonated forms, become positive under the solvent effect and depend on the nature of protonation. Like for phenazine and related compounds theoretical inhibitory study by Ebenso et al., we can conclude in light of protonated forms quantum chemical parameters results of our molecules, that the protonated forms are more reactive than neutral forms by receiving electrons from the metal surface, however the solvent moderates their reactivity [58,59].

### 3.3.2. Preferred sites of protonation and solvent effect

The preferred site for protonation is determined by comparing the proton affinity PA at the different possible sites. Based on the equation (12) and knowing that  $E_{1\text{MCTH}} = -1275,009$  hartree;  $E_{2\text{MCTH}} = -1429,127$  hartree;  $E_{\text{H}_2\text{O}} = -76,728$  hartree and  $E_{\text{H}_3\text{O}^+} = -76,452$  hartree, the PA is evaluated and presented in Tab. 6. The calculations show that the protonation process is exothermic, meaning that all inhibitors have a tendency for protonation. Moreover, it has reported that the more negative the value of PA, the more inhibiting effect increases because it's related to its basicity. The PA values, for both 1MCTH and 2MCTH, have shown that the double protonation on nitrogen atoms N9 and N10, is preferred than a double protonation on oxygen atoms O26 and O27 (Figure.7). Furthermore, the protonation on N9 or N10 is preferred than those on O26 or O27. Moreover, the aqueous solvation has a stabilizing effect on the protonation process and preserves the same order of protonation preference.

It should be noted that, in the presence of aqueous solvent or not, the sulfur has the least stable protonation, which is in agreement with 1MCTH and 2MCTH global and local electronic proprieties, for which the sulfur is only able to receive electrons. Note that it's widely thought that molecules with N atoms are preferentially protonated in acidic medium while molecules with S and O atoms do not prefer to undergo protonation [59].

Some protonated inhibitors	HOMO	T.D. HOMO	LUMO	T.D. LUMO
1MCTHN <sub>9</sub> H+N <sub>10</sub> H+				
1MCTHO <sub>26</sub> H+O <sub>27</sub> H+				
2MCTHN <sub>9</sub> H+N <sub>10</sub> H+				
2MCTHO <sub>26</sub> H+O <sub>27</sub> H+				

**Figure 6.** HOMO, LUMO and total density charge (T.D) of some protonated inhibitors 1-MCTH and 2-MCTH optimized structures in vacuo at B3LYP/6-31G\*\*.

### 3.3.3. Selected geometrical parameters of isolated favoured protonated species and in aqueous Solution

The variations of some selective geometrical parameters between the neutral species and the preferred protonated species are reported in Table. 1. Such a comparison shows the effect of protonation on the geometry. For 1-MCTH, the double protonation on N9-N10 decreases C3-C6 and C11-C8 of about 0.04 Å, increases C6-N9 and C8-N10 of about 0.03 Å and decreases C24-C25 distance of about 0.12 Å, while the double protonation on O26-O27 increases remarkably C24-O26 and C25-O27 of about 0.1 Å and C24-C25 distance of about 0.22 Å reducing aryls interaction.

The torsional angles between the two aromatic rings, expressed by C20-C3-C11-C22 or C16-C24-C25-C18 is shorter in 1-MCTHN<sub>9</sub>H+N<sub>10</sub>H+ and 1-MCTHO<sub>26</sub>H+O<sub>27</sub>H+ by about 8° than in

than 1-MCTH, while the torsional angle between the thiadiazole ring and the aromatic rings, expressed by C24-C3-C6-S7 or C25-C11-C8-S7 is shorter for 1-MCTHN9H+N10H<sup>+</sup> by about 20°, but larger by 5° and 12° respectively for 1MCTHO26H+O27H<sup>+</sup> than in 1-MCTH, suggesting that the degree of planarity is enhanced by protonation of the nitrogens compared to oxygens protonation.

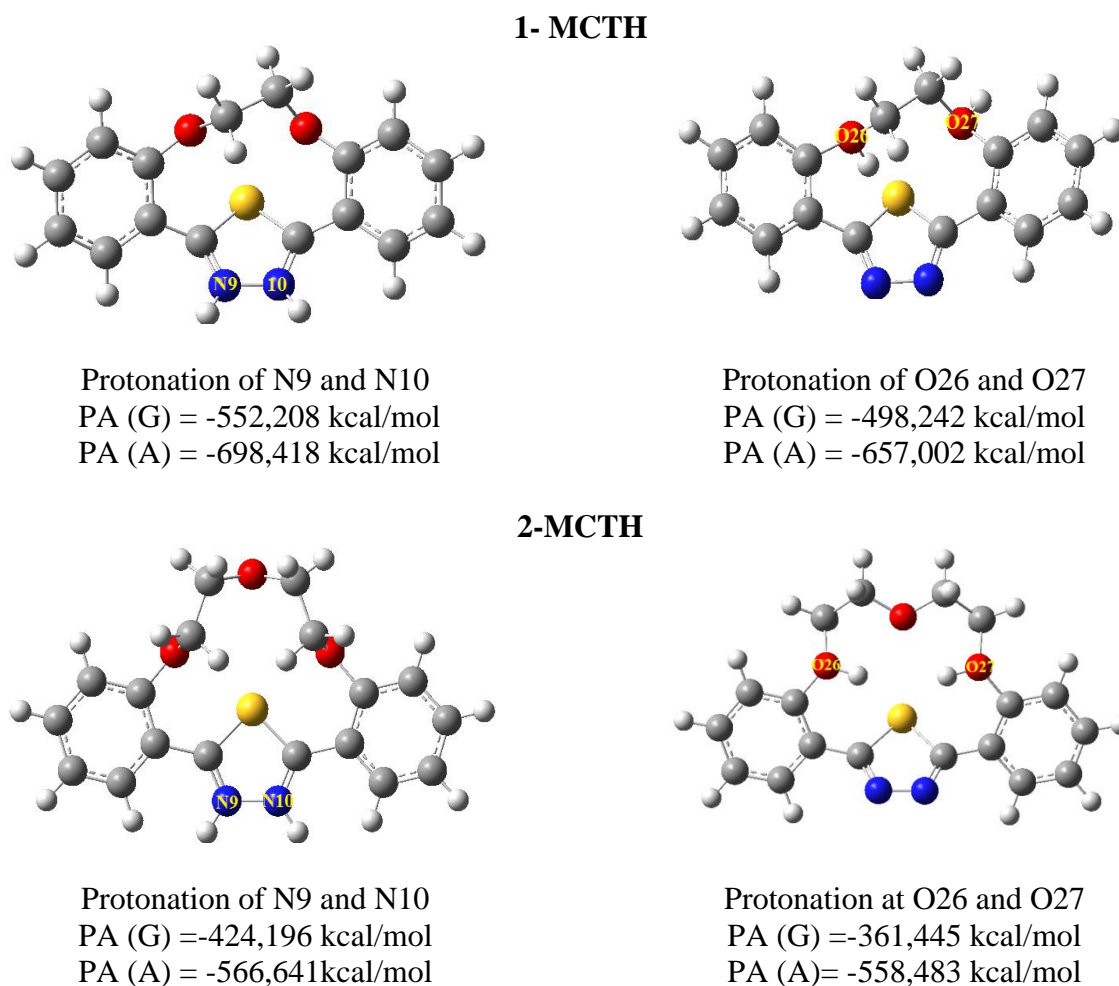


**Figure 7** . The double protonated species of 1-MCTH and 2-MCTH in vacuo (G) and in aqueous solution (A) at B3LYP/6-31G\*\* and the corresponding proton affinity values (kcal/mol).

For 2-MCTH, the N9-N10 double protonation decreases C3-C6 and C11-C8 of about 0.04 and increases C6-N9, C8-N10 and N9-N10 of about 0.04 Å. A significant decreases were noted for C24-O26 and C25-O27 (by 0.1 Å) and for C24-C25 distance (by 0.14 Å), the distance between thiadiazole sulfur and oxygens O26 and O27 is decreased by 0.3 Å. The torsional angle between the thiadiazole ring and the aromatic rings, expressed by C24-C3-C6-S7 or C25-C11-C8-S7 is reduced to almost 0° integrating the thiadiazole in the same plane as aromatic rings, giving this cation a high degree of planarity. The double protonation on O26-O27 increases C24-O26 and C25-O27 of about 0.03, C24-C25 distance by 0.06 and C35-O26 with C32-O27 of about 0.08 Å. Its most notable change concerns

the couple of interatomic distances (N9-O26, N10-O27) which decreases of about 0.23 Å and (S7-O26, S7-O27) which increases by 0.37 Å, suggesting hydrogen bond between hydrogen of protonated oxygen and nitrogen. Indeed, the increase of C24-C3-C6-S7 or the decrease of C25-C11-C8-S7 by 65° is a tangible confirmation. Thereby, unlike the double protonation on N9-N10, the double protonation on O26-O27 acts against the planarity of thiadiazole ring with respect to aryl segments, thus against the planarity of the inhibitor. Based on C24-C3-C6-S7 (or C2-C11-C8-S7) and C20-C3-C11-C22 (or C18-C25-C24-C16) torsional angle values after solvation of double nitrogen protonated species, we have found that the degree of planarity has not been substantially affected for both 1-MCTH and 2-MCTH. However, the double protonation, for 2-MCTH, on O26-O27, consolidate the hydrogen bond, causing thus an inversion of the thiadiazole ring as C24-C3-C6-S7 increases of about 95°. Thus, it could be concluded that 2-MCTHN9H+N10H+, which has the highest degree of planarity is more favorable, in term of reactivity with metallic surface, than the other protonated forms (Fig.8), knowing that it's more reactive than 2-MCTH in terms of electron reception from the metal surface. It should be emphasized that sometimes the geometric planarity rivals the electron density of the inhibitors. In this case, like the quinolone derivatives inhibitors studied by Ebenso for mild steel in acidic medium, priority is given to the last factor [60].

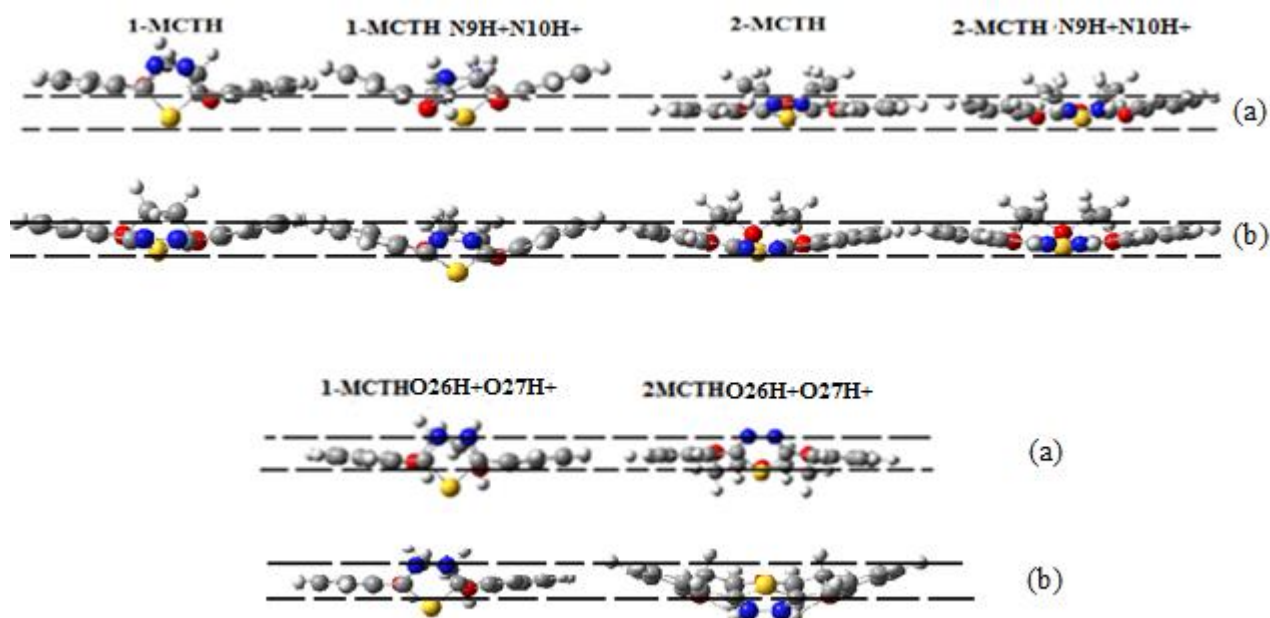


**Figure 8.** Planarity influencing factor in neutral inhibitors 1-MCTH and 2-MCTH and their double protonated forms: (a) *in vacuo* (*G*) and (b) *in aqueous solution* (*A*) at B3LYP/6-31G\*\*.(The region between the dotted lines represents the surface of the iron metal).

### 3.3.4. Molecular electrostatic potential of isolated favored protonated species

Through the evaluation of the molecular electrostatic potential, it's possible to determine the degree of activity of 1-MCTHN9H+N10H+ and 2-MCTHN9H+N10H+. Their MEP surface picture,

given in Figure 5, reveals that, the region of high negative charges seen around N9 and N10 for the neutral species disappears entirely as the red color is replaced by blue one. This phenomenon is a result of the high electronegative charge of the N atom which leaves the H atom deficient in electrons, strongly attached to it. This confirms the ability of the protonated forms to receive electrons from the metallic surface instead of giving them, as can be seen for quinolone derivatives protonated forms [60].

**Table 6.** Interaction energies with iron surface of the B3LYP/6-31G\*\*neutral inhibitors 1-MCTH and 2-MCTH optimized structures and their optimized double nitrogen protonated forms *in vacuo* (G).

<b>Complexes</b>	<b>Fe</b>	<b>1-MCTH</b>	<b>Fe-N<sub>9</sub></b>	<b>Fe-N<sub>10</sub></b>	<b>Fe-(N<sub>9</sub>N<sub>10</sub>)</b>
Total Energy (a.u.)	-123.253	-1275.009	-1398.299	-1398.300	-1398.316
Interaction Energy (a.u.)	-	-	0.037	0.038	0.054
Interaction Energy(kcal/mol)	-	-	23.262	23.997	33.930
<b>Complexes</b>	<b>Fe</b>	<b>2-MCTH</b>	<b>Fe-N<sub>9</sub></b>	<b>Fe-N<sub>10</sub></b>	<b>Fe-(N<sub>9</sub>N<sub>10</sub>)</b>
Total Energy (a.u.)	-123.253	-1440.57	-1563.869	-1563.869	-1563.899
Interaction Energy (a.u.)	-	-	0.043	0.043	0.073
Interaction Energy(kcal/mol)	-	-	26,714	26,714	45,539
<b>Complexes</b>	<b>Fe</b>	<b>1MCTHN<sub>9</sub>H+N<sub>10</sub>H+</b>	<b>Fe-N<sub>9</sub></b>	<b>Fe-N<sub>10</sub></b>	<b>Fe-(N<sub>9</sub>N<sub>10</sub>)</b>
Total Energy (a.u.)	-123.253	-1275.613	-1398.891	-1398.897	-1398.910
Interaction Energy (a.u.)			0.025	0.031	0.044
Interaction Energy(kcal/mol)			15,544	19,196	27,423
<b>Complexes</b>	<b>Fe</b>	<b>2MCTHN<sub>9</sub>H+N<sub>10</sub>H+</b>	<b>Fe-N<sub>9</sub></b>	<b>Fe-N<sub>10</sub></b>	<b>Fe-(N<sub>9</sub>N<sub>10</sub>)</b>
Total Energy (a.u.)	-123.253	-1440.79	-1564.079	-1564.079	-1564.109
Interaction Energy (a.u.)			0.033	0.033	0.063
Interaction Energy(kcal/mol)			20.439	20.439	39.264

### 3.4. Metal-inhibitor interaction mechanism *in vacuo* and *in solvent effect*

After having located the most active sites (nitrogens) in both neutral and protonated forms of 1-MCTH and 2-MCTH and with the aim of approaching their interaction strength with iron and in order to further elucidate the mode of action of both forms, we attempted to quantify their interaction with the iron in the metallic complex. To this end, two calculation methods have been considered:

- The interaction of 1-MCTH (1-MCTN<sub>9</sub>H+N<sub>10</sub>H<sup>+</sup>) and 2-MCTH (2-MCTHN<sub>9</sub>H+N<sub>10</sub>H<sup>+</sup>) with one iron atom was studied by DFT as a model for a corrosion inhibition process.

- The dynamic Monte Carlo (MC) simulation was adopted to look for the lowest configuration adsorption energy of the interactions of 1-MCTH, 2-MCTH and their double nitrogen protonated forms on the iron surface, represented by Fe (111) plane, with and without solvent [42].

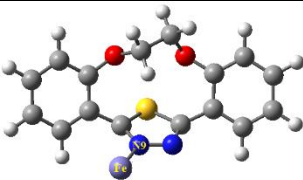
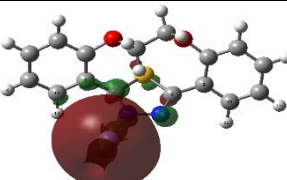
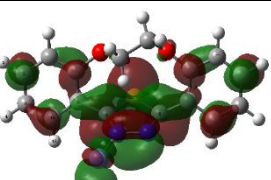
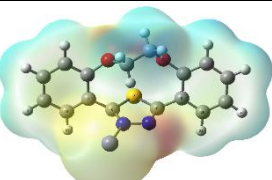
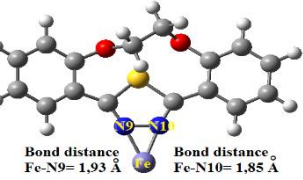
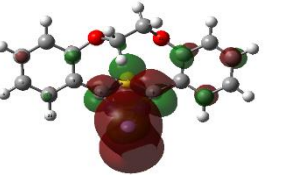
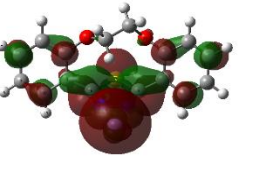
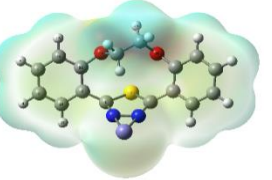
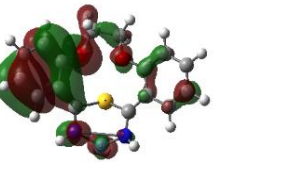
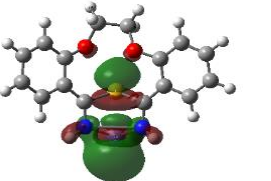
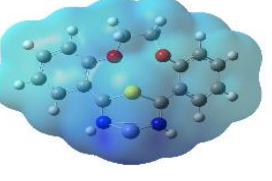
The interaction energy between the inhibitor and the metal was then estimated as the difference between the energy of the complex ( $E_{\text{total}}$ ) and the sum of the isolated inhibitor energy and isolated Fe atom or Fe surface energy, resulting in the equation:

$$E_{\text{interaction}} = E_{\text{total}} - (E_{\text{inhibitor}} + E_{\text{Fe/surface}}) \quad (18)$$

The binding energy equals the negative value of the interaction energy

$$E_{\text{binding}} = - E_{\text{interaction}} \quad (19)$$

Figure 9 shows also HOMO, LUMO and total electron density for the Fe-inhibitor complexes. As can be seen, for both 1MCTH and 2MCTH, the interaction of iron atom with two nitrogens stabilizes better the complex compared to the interaction with one nitrogen, confirming Table 7 results.

1-MCTH/N <sub>9</sub> -Fe	HOMO	LUMO	Total charge density
 Bond distance Fe-N <sub>9</sub> = 1,84 Å			
1-MCTH/(N <sub>9</sub> N <sub>10</sub> )-Fe	HOMO	LUMO	Total charge density
 Bond distance Fe-N <sub>9</sub> = 1,93 Å    Bond distance Fe-N <sub>10</sub> = 1,85 Å			
1-MCTHN <sub>9</sub> H+N <sub>10</sub> H <sup>+</sup> /(N <sub>9</sub> N <sub>10</sub> )-Fe	HOMO	LUMO	Total charge density
 Bond distance N <sub>9</sub> -Fe= 1,887 Å; N <sub>10</sub> -Fe = 1,895 Å			
2-MCTH/N <sub>9</sub> -Fe	HOMO	LUMO	Total charge density

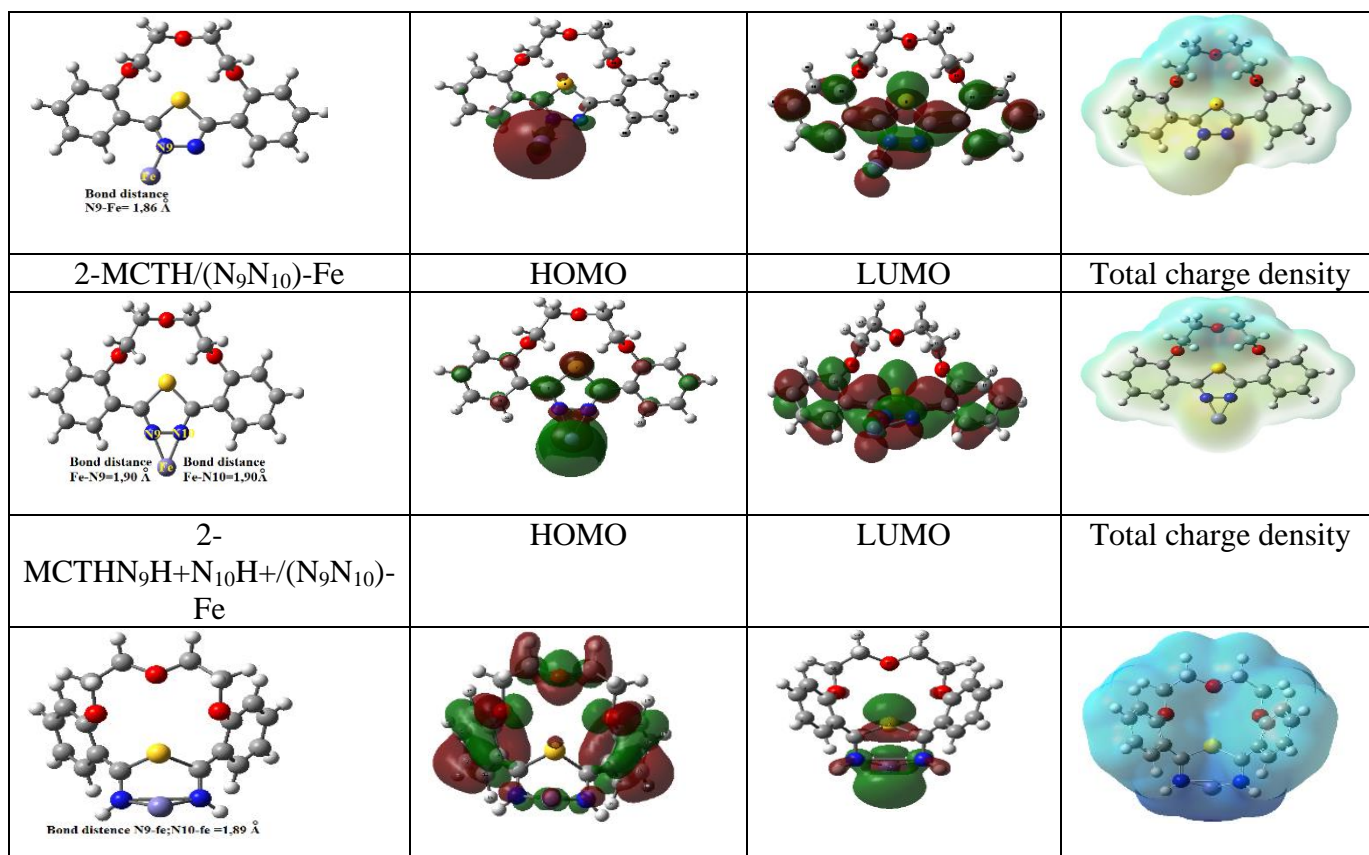


**Figure 9.** The optimized structures, HOMO, LUMO and total charge density (T.D) of Fe-inhibitor complexes and Fe-protonated inhibitor complexes in vacuo.

### 3.4.1. DFT calculation of complexation

Neutral forms 1MCTH, 2MCTH and their nitrogen doubly protonated form 1MCTH(NH<sup>+</sup>)<sub>2</sub> (2MCTH(NH<sup>+</sup>)<sub>2</sub>) were allowed to interact, at nitrogen atoms, with the Fe metal, reduced to a single iron atom. The interaction energy between the metal and the inhibitor is reported in Table 7. From this table, it is clear that the interaction involving one nitrogen is less than that involving two nitrogens. Moreover, the table shows, for each molecule, the importance of the interaction involving neutral form compared to protonated one. In this regard, the adsorption of inhibitors over metal surface may happen in two different ways: chemical adsorption (electron-sharing between the inhibitor molecule *n*-MCTH and the metal) and/or Physical adsorption (electrostatic interaction between the charged inhibitor *n*-MCTH(NH<sup>+</sup>)<sub>2</sub> and Fe surface) [3]. Supported by the histogram of Figure.10, Table 7 shows also the supremacy of the Fe-(N<sub>9</sub>N<sub>10</sub>)-like interaction involving 2-MCTH as the strength follows the order: 2-MCTH > 2-MCTH(NH<sup>+</sup>)<sub>2</sub> > 1-MCTH > 1-MCTH(NH<sup>+</sup>)<sub>2</sub>. It's worth noting that the supremacy of iron atom interaction energy with neutral form compared to protonated ones depends on the nature of the inhibitor since Hadi Behzadi et al found the opposite of our results for pyrazine derivatives-Fe complexes in corrosion inhibition theoretical investigation [61]. However, these results aren't supported by the totality of N-Fe bond distances (Figure.10) which should decrease with the interaction strength. This is probably due to the orientation of the iron atom relative to nitrogen during

the optimization process and the need to consider an iron atom cluster instead of one atom (Fen, n:1-4 atoms), like the work done by D. Turcio-Ortega et al. on imidazoline compounds complexation with iron atoms [62].

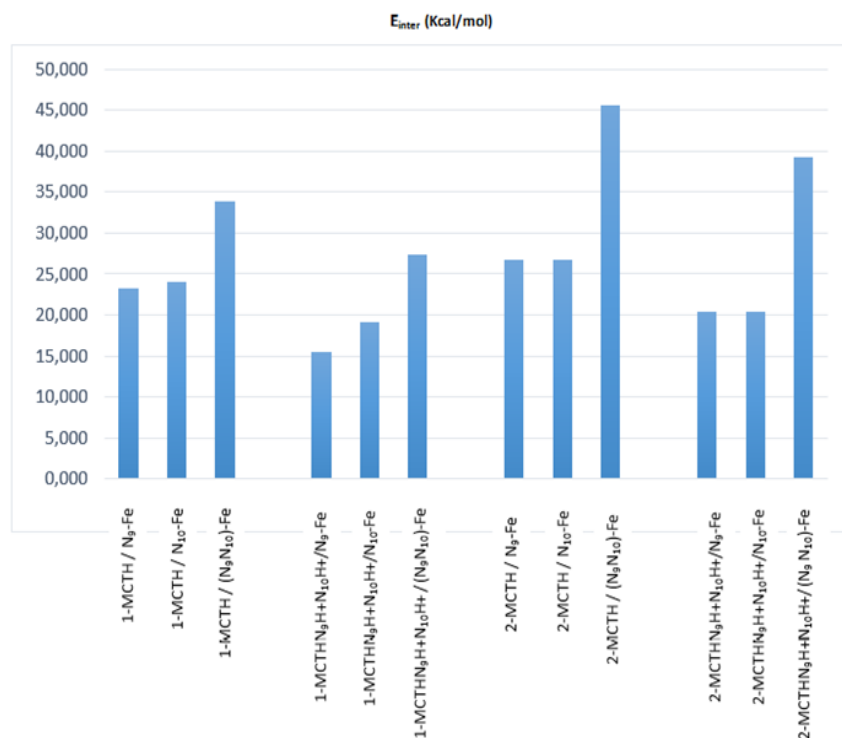


**Figure 10.** Interaction energies with iron surface of the B3LYP/6-31G\*\*neutral inhibitors 1-MCTH and 2-MCTH optimized structures and their optimized double nitrogen protonated forms, in vacuo (G).

Indeed, the HOMO are more delocalized throughout the complex when iron is double bounded with nitrogens. Fig. 8 also confirm the stabilizing effect of Fe-(N<sub>9</sub>N<sub>10</sub>) interaction in 2-MCTH-Fe complex compared to 1-MCTH-Fe as well as in 2-MCTH(NH<sub>2</sub>)<sub>2</sub>-Fe compared to 1-MCTH(NH<sub>2</sub>)<sub>2</sub>-Fe. Indeed, the LUMO of 2-MCTHNN-Fe is more delocalized than the LUMO of 1-MCTHNN-Fe and the HOMO of 2-MCTH(NH<sub>2</sub>)<sub>2</sub>-Fe is more delocalized compared to 1-MCTH(NH<sub>2</sub>)<sub>2</sub>-Fe complex. Moreover, the electron density potential surface shows that there is a relatively negative charge (indicated by the red color) on the nitrogen not involved in the complexation compared to the nitrogen bounded to iron, showing the stabilizing effect of the complexation on nitrogens. The comparison of the molecular quantum descriptors of the complexes formed is an additional confirmation (Table 8). Among those is, for example  $\Delta E$ , as the highest  $\Delta E$  value corresponds to the least reactive complex, leading 2-MCTH-Fe and 2-MCTH(NH<sub>2</sub>)<sub>2</sub>-Fe complexes least reactive than 1-MCTH-Fe and 1-MCTH(NH<sub>2</sub>)<sub>2</sub>-Fe, respectively.

## 3.4.2. Dynamic Monte Carlo study of complexation

The adsorption energy, evaluating the primary mechanism of corrosion inhibitor interaction with iron, can be calculated by dynamic Monte Carlo simulation. It represents a direct tool to classify the efficiency of the studied inhibitors. The total energy is defined as the sum of the energies of the adsorbate components while the total adsorption energy is defined as the sum of the rigid adsorption energy and the deformation energy. Both total energy, collective adsorption energy, individual adsorption energy of inhibitor ( $dE_{\text{ads}}/dN_{\text{inhibitor}}$ ) and that of H<sub>2</sub>O molecule ( $dE_{\text{ads}}/dN_{\text{H}_2\text{O}}$ ) [39,40] were calculated and presented in Table 9.

**Table 7.** Some optimized quantum chemical parameters for Fe-inhibitor complexes and Fe-protonated inhibitor complexes in vacuo (G).

	$E_{\text{HOMO}}$	$E_{\text{LUMO}}$	$\mu$	$\Delta E$	X	$\eta$	$\Omega$
<b>Fe-inhibitor complexes</b>							
1-MCTH / N <sub>9</sub> -Fe	-7.341	-2.319	3.750	5.021	5.990	6.181	2.903
1-MCTH / N <sub>10</sub> -Fe	-7.363	-2.316	3.690	5.046	5.998	6.205	2.899
1-MCTH / (N <sub>9</sub> N <sub>10</sub> )-Fe	-7.425	-2.192	3.200	5.233	5.904	6.329	2.754
2-MCTH / N <sub>9/10</sub> -Fe	-7.396	-2.262	3.241	5.134	5.960	6.265	2.835
2-MCTH / (N <sub>9</sub> N <sub>10</sub> )-Fe	-7.498	-2.122	3.194	5.376	5.871	6.437	2.678
<b>Fe-protonated inhibitor complexes</b>							
1-MCTHN <sub>9</sub> H+N <sub>10</sub> H+/ N <sub>9</sub> -Fe	-13.153	-8.821	5.650	4.332	15.398	8.821	13.439
1-MCTHN <sub>9</sub> H+N <sub>10</sub> H+/ N <sub>10</sub> -Fe	-13.179	-8.829	5.540	4.350	15.419	8.829	13.463
1-MCTHN <sub>9</sub> H+N <sub>10</sub> H+/ (N <sub>9</sub> N <sub>10</sub> )-Fe	-13.291	-8.803	4.610	4.488	15.448	8.803	13.556
2-MCTHN <sub>9</sub> H+N <sub>10</sub> H+/ N <sub>9/10</sub> -Fe	-13.222	-8.809	4.830	4.413	15.420	8.809	13.497
2-MCTHN <sub>9</sub> H+N <sub>10</sub> H+/ (N <sub>9</sub> N <sub>10</sub> )-Fe	-13.381	-8.800	4.440	4.581	15.490	8.800	13.634

All energy values are in eV;  $\mu$ : the dipole moment in Debye; S: the global softness in  $\text{eV}^{-1}$ .

The Figure 11 shows the equilibrium adsorption configurations of the neutral forms 1MCTH (2MCTH) and double protonated ones 1-MCTH(NH<sub>2</sub>)<sub>2</sub> (2MCTH(NH<sub>2</sub>)<sub>2</sub>) in vacuo and in aqueous solution. Based on the collective adsorption energy and individual adsorption energy values of the inhibitor, the classification of the interaction strength of (111) surface-inhibitor systems reproduces, both in vacuo and in aqueous phase, the same order as the DFT calculation of binding energies for iron complexes.

Moreover, the direct correlation between the interaction strength of (111) surface-inhibitor systems and the distance between nitrogens and the nearest Fe atom, collected in Tab. 10, consolidates these results. It's worthwhile noticing that only the distance N-Fe for 2MCTH is below the threshold of 3Å, suggesting that the adsorption is chemical. On the other hand, it can be seen from Table.9 that

water adsorption remains very low compared to the inhibitor adsorption. This favors the gradual substitution of water molecules from the iron surface by inhibitor components, resulting in the formation of a stable layer which can protect the iron from aqueous corrosion. Some structural parameters variations of 1-MCTH-Fe and 2-MCTH-Fe from DFT to dynamic Monte Carlo computations were noticed (Table 11).

**Table 8.** Outputs and descriptors for the lowest adsorption configurations for (1-MCTH and 2-MCTH) on Fe (111) surface. Calculated by Monte Carlo simulation in gas and aqueous phase. (All values in kcal/mol).

Systems	Total energy	Adsorption energy	Rigid adsorption energy	Deformation energy	dEad/dNi inhibitor	dEad/dNi H2O
<b>Fe(111)-inhibitor complexes</b>						
Fe(111)/1-MCTH	29.820	-156.729	-121.959	-24.770	-146.729	-
Fe(111)/2-MCTH	-25.627	-468.904	-156.280	-313.620	-455.834	-
Fe(111)/1-MCTH/50 H <sub>2</sub> O	- 355.163	-542.589	-435.671	-20.051	-143.272	-14.240
Fe(111)/2-MCTH/50 H <sub>2</sub> O	- 386.200	-840.347	-529.583	-310.763	-467.587	-7.246
<b>Fe(111)-protonated inhibitor complexes</b>						
Fe(111)/1-MCTH(NH <sub>2</sub> ) <sub>2</sub>	32.32	-152.745	-118.256	-21.335	-143.234	-
Fe(111)/2-MCTH(NH <sub>2</sub> ) <sub>2</sub>	-22.425	-464.642	-153.849	-310.291	-465.078	-
Fe(111)/1-MCTH(NH <sub>2</sub> ) <sub>2</sub> /50 H <sub>2</sub> O	- 350.592	-538.773	-430.983	-18.735	-140.174	-12.734
Fe(111)/2-MCTH(NH <sub>2</sub> ) <sub>2</sub> /50 H <sub>2</sub> O	- 381.375	-836.879	-524.293	-307.982	-463.753	-5.859

Indeed, the bond lengths or atomic distances decreased of about 0.02Å. Concerning the torsional angles, the variation doesn't exceed 4° for 1-MCTH-Fe while it's almost zero for 2-MCTH-Fe. In this context, we have pointed out that NN bond length increases from the inhibitor (1-MCTH or 2-MCTH) to DFT complex of 0.06 Å and to MC complex of 0.04 Å. The resulting weakness of NN bond is certainly caused by the strengthening of N-Fe interaction, an additional argument for considering chemical adsorption for neutral forms.

In the light of molecular dynamic study, we point out that 2-MCTH, in its neutral or double nitrogen protonated forms, were adsorbed much better than 1-MCTH or its double nitrogen protonated form respectively, which explains its highest inhibition efficiency compared to 1-MCTH. Indeed, the high degree of planarity of 2-MCTH compared to 1-MCTH strengthens the adhesion of the molecule

on the surface from a dynamic as well as a quantum point of view, like the dynamic and quantic results comparing the inhibition efficiency of 1,18-diaza-(3,4;15,16;- dibenzo)-19,27-oxydianiline-5,8,11,14-tetra oxa cycloheptacosine-1,17-diene noted L and 1,10 - bis(2-formylphenyl)-1,4,7,10- tetraoxadecane noted Ald, knowing that the former presents macrocyclic polyether cavity favouring the relative planarity of the molecule [55].

**Table 9.** The distance between Nitrogens and the nearest Fe atom of Fe (111) surface

	1MCTH-Fe	1MCTH(NH+)2-Fe	2MCTH-Fe	2MCTH(NH+)2-Fe
Fe-N*	3.25	3.40	2.98	3.07
Fe-N*/50H <sub>2</sub> O	3.38	3.41	2.99	3.10

\*When N9 and N10 are not equivalent, the distance considered is that separating the nearest Fe atom to the middle of the NN bond.

**Table 10.** Bond distance (Å) and torsional angle (°) for the B3LYP/6-31G\*\* optimized complexes of 1-MCTH and 2-MCTH with Fe, in aqueous solution (A), calculated by B3LYP/6-31G\*\* and dynamic Monte Carlo simulation.

Bond	1-MCTHNN-Fe	1-MCTHNN-Fe	2-MCTHNN-Fe	2-MCTHNN-Fe
	(A) DFT	(A) MC	(A) DFT	(A) MC
C3-C6	1.465	1.441	1.452	1.428
C6-S7	1.835	1.811	1.843	1.819
C8-S7	1.841	1.817	1.843	1.819
C6-N9	1.319	1.295	1.329	1.305
C8-N10	1.339	1.315	1.329	1.305
C8-C11	1.456	1.432	1.452	1.428
C24-O26	1.409	1.385	1.412	1.388
C25-O27	1.410	1.386	1.412	1.388
N9-N10	1.430	1.406	1.408	1.384
S7-O26	3.071	3.047	2.794	2.770
S7-O27	2.923	2.899	2.794	2.770
N9-O26	3.861	3.837	4.227	4.203
N10-O27	3.975	3.951	4.227	4.203
C24-C25	5.338	5.314	6.475	6.451
C3-C11	5.138	5.114	5.390	5.366
O26-C28	1.478	1.454	-	-
O27-C31	1.473	1.449	-	-
O26-C35	-	-	1.474	1.450
O27-C32	-	-	1.474	1.450
Torsional angle	1-MCTH-Fe (A) DFT	1-MCTH-Fe (A) MC	2-MCTH-Fe (A) DFT	2-MCTH-Fe (A) MC
C24-C3-C6-S7	-49.938	-46.453	-10.431	-10.212
C25-C11-C8-S7	39.081	35.526	-10.431	-10.212
C20-C3-C11-C22	-19.710	-18.246	0.000	0.000

C18-C25-C24-C16	18.248	16.367	0.000	0.000
O26-N9-N10-O27	-5.694	-5.268	0.000	0.000
C3-O26-O27-C11	-19.716	-17.725	0.000	0.000
C24-O26-O27-C25	-40.950	-38.862	0.000	0.000
C28-N9-N10-C31	-6.804	-6.035	0.000	0.000

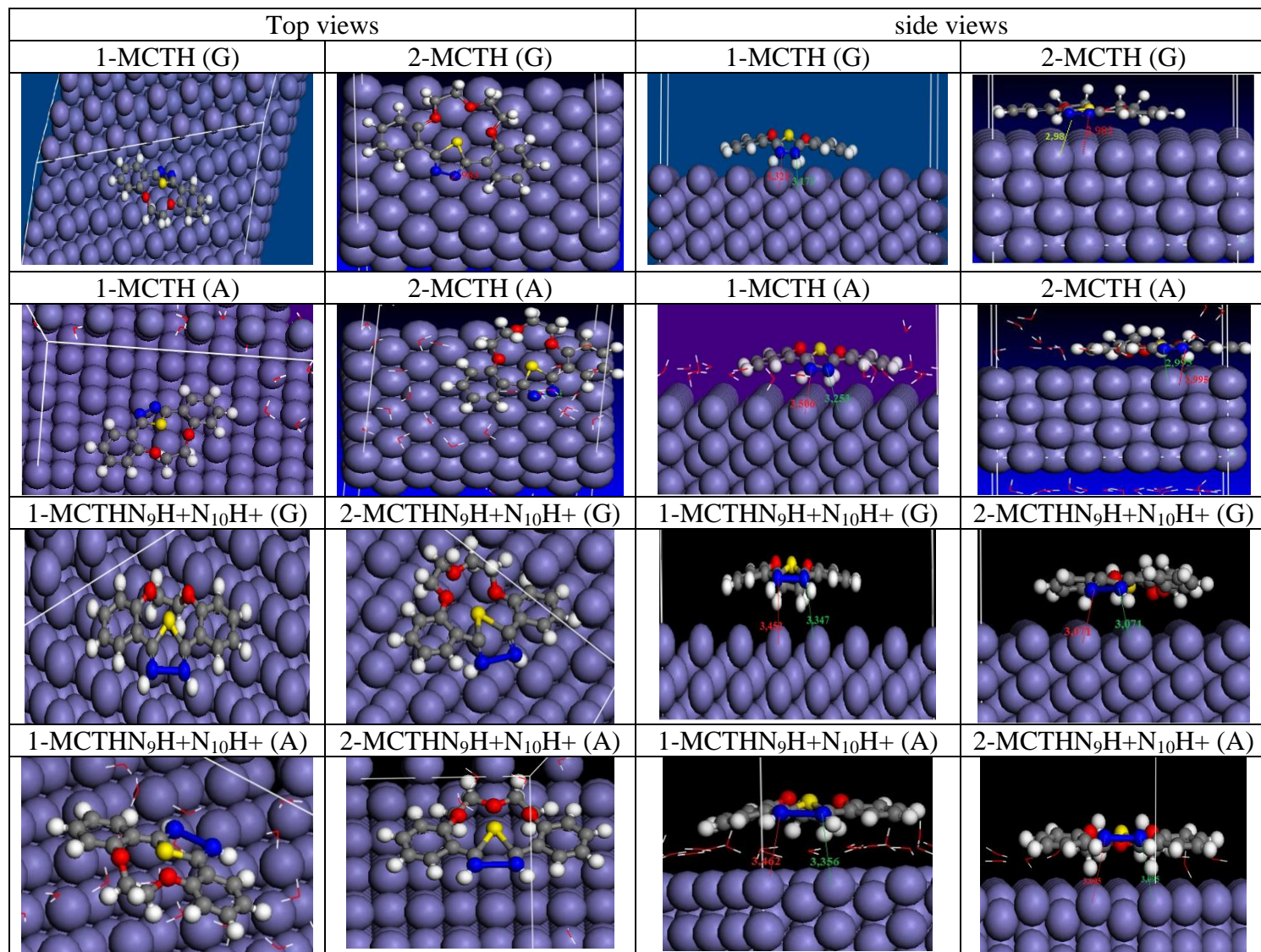


**Figure 11.** Top and side views of stable adsorption configurations of 1-MCTH, 2-MCTH, 1-MCTH(NH<sup>+</sup>)<sub>2</sub> and 2-MCTH(NH<sup>+</sup>)<sub>2</sub> inhibitors on Fe (111) iron surface in vacuo (G) and aqueous phase (A) (50 H<sub>2</sub>O).

#### 4. CONCLUSIONS

The following conclusion made based on large theoretical and comparative study:

- ❖ 2-MCTH is found more planar and more reactive in donating and accepting electron process compared to 1-MCTH.
- ❖ The evaluation of proton affinity energy led to N9 and N10 as the preferred sites of protonation.
- ❖ The 2-MCTH double protonated form on nitrogens, is more planar and more able to receive electrons from the metal surface, compared to the other protonated and neutral forms.
- ❖ Both DFT and dynamic Monte Carlo studies of iron complexation, in vacuo and aqueous phase, led to the supremacy of the Fe-(N9N10)-like interaction involving 2-MCTH, with the interaction strength obeying the following order: 2-MCTH > 2-MCTH(NH<sup>+</sup>)<sub>2</sub> > 1-MCTH > 1-MCTH(NH<sup>+</sup>)<sub>2</sub>.
- ❖ The distance N-Fe for 2-MCTHNN-Fe complex is below the threshold of 3 Å, suggesting that the adsorption is chemical.
- ❖ As expected, this work supports the experimentally inhibition efficiency results collected in Table 2. Our plane, as a perspective, to consider an iron atom cluster instead of one atom (Fe<sub>n</sub>, n:1-4 atoms) with more advanced quantum methods and the oxidized iron Fe<sub>2</sub>O<sub>3</sub> surface models for molecular dynamics study. We will extend also our study to comparable molecules, especially 3-MCTH, 4-MCTH and 5-MCTH to prove that 5-MCTH is the most efficient corrosion inhibitor.

#### ACKNOWLEDGMENT

We thank Dr. F. Bentiss for showing us the experimental interest of the studied molecules.

#### References

1. G. E. Badr, *Corros. Sci.*, 51 (2009) 2529.
2. D. Asefi, M. Arami, and N. M. Mahmoodi, *Corros. Sci.*, 52 (2010) 794.
3. K. Zhang, B. Xu, W. Yang, X. Yin, Y. Liu, and Y. Chen, *Corros. Sci.*, 90 (2015) 284.
4. N. Anusuya, J. Saranya, P. Sounthari, A. Zarrouk, and S. Chitra, *J. Mol. Liq.*, 225 (2017) 406.
5. C. M. Goulart, A. Esteves-Souza, C. A. Martinez-Huitle, C. J. F. Rodrigues, M. A. M. Maciel, and A. Echevarria, *Corros. Sci.*, 67 (2013) 281.
6. D. Özkir, K. Kayakirilmaz, E. Bayol, A. A. Gürten, and F. Kandemirli, *Corros. Sci.*, 56 (2012) 143.
7. S. Benabid, T. Douadi, S. Issaadi, C. Penverne, and S. Chafaa, *Meas. J. Int. Meas. Confed.*, 99 (2017) 53.
8. A. Zarrouk, B. Hammouti, A. Dafali, M. Bouachrine, H. Zarrok, S. Boukhris and S. S. Al-Deyab, *J. Saudi Chem. Soc.*, 18 (2014) 450.
9. F. Bentiss, M. Lebrini, H. Vezin, and M. Lagrenée, *Mater. Chem. Phys.*, 87 (2004) 18.
10. M. Lebrini, Synthèse et études physico-chimiques de nouveaux thiadiazoles inhibiteurs de corrosion de l'acier en milieu acide, University thesis N° ordre 3659, University sciences et technologie de Lille 1, Lille, France, 2005.
11. M. Lebrini, M. Lagrene, H. Vezin, M. Traisnel, F. Bentiss, *Corros. Sci.*, 49 (2007) 2254.
12. F. Bentiss, M. Lebrini, H. Vezin, F. Chai, M. Traisnel, and M. Lagrené, *Corros. Sci.*, 51 (2009) 2165.
13. A. Mahsoun, K. Sadik, M. Elalaoui Belghiti, I. Bahadur, Aboulmouhajir, *Int. J. Electrochem. Sci.*, 13 (2018) xx.

14. A. S. Thomas, Z. Nahossé and B. Kafoumba, *European scientific journal*, 11 (2015) 148.
15. D. Gopi, E. S. M. Sherif, M. Surendiran, M. Jothi, P. Kumaradhas, and L. Kavitha, *Mater. Chem. Phys.*, 147 (2014) 572.
16. L. R. Domingo and P. Pérez, *Org. Biomol. Chem.*, 11 (2013) 4350.
17. K. Vanasundari, V. Balachandran, M. Kavimani, and B. Narayana, *J. Mol. Struct.*, 1147 (2017) 136.
18. J. Luo, Z. Xue, W. Liu, J. Wu, and Z. Yang, *J. Phys. Chem. A*, 110 (2005) 12005.
19. M. Elbelghiti, Y. Karzazi, A. Dafali, B. Hammouti, F. Bentiss, I. B. Obot, I. Bahadur, E. E. Ebenso, *J. Mol. Liq.*, 218 (2016) 281.
20. V. S. Sastri and J. R. Perumareddi, *Corrosion*, 53 (1997) 617.
21. M. Abd El-Raouf, E. A. Khamis, M. T. H. Abou Kana, and N. A. Negm, *J. Mol. Liq.*, 255 (2018) 341.
22. A. Singh, K. R. Ansari, J. Haque, P. Dohare, H. Lgaz, R. Salghi, M. A. Quraishi, *J. Taiwan Inst. Chem. Eng.*, 82 (2018) 233.
23. S. I. Kiyooka, D. Kaneno, and R. Fujiyama, *Tetrahedron Lett.*, 54 (2013) 339.
24. T. C. Allison and Y. J. Tong, *Electrochim. Acta*, 101 (2013) 334.
25. Z. Cao, Y. Tang, H. Cang, J. Xu, G. Lu, and W. Jing, *Corros. Sci.*, 83 (2014) 292.
26. M. Kavimani, V. Balachandran, B. Narayana, K. Vanasundari, and B. Revathi, *Spectrochim. Acta Part A Mol. Biomol. Spectrosc.*, 190 (2018) 47.
27. Z. R. Grabowski, K. Rotkiewicz, and W. Rettig, *Chem. Rev.*, 103 (2003) 3899.
28. S. Sakthivel, T. Alagesan, S. Muthu, C. Susan, and E. Geetha, *J. Mol. Struct.*, 1156 (2018) 645.
29. S. P. Vijayachamundeeswari, B. Yagna Narayana, S. Jone Pradeepa, and N. Sundaraganesan, *J. Mol. Struct.*, 1099 (2015) 633.
30. A. E. Reed, L. a Curtiss, and F. Weinhold, *Chem. Rev.*, 88 (1988) 899.
31. I. B. Obot, E. E. Ebenso, and M. M. Kabanda, *J. Environ. Chem. Eng.*, 1 (2013) 431.
32. E. D. Raczyńska, M. Makowski, E. Górnicka, and M. Darowska, *Int. J. Mol. Sci.*, 6 (2005) 143.
33. L. H. Madkour, S. Kaya, and I. B. Obot, *J. Mol. Liq.*, x (2018) x.
34. M. Bourass, A. Touimi Benjelloun, M. Benzakour, M. Mcharfi, F. Jhilal, F. Serein-Spirau, J. Marc Sotiropoulos, M. Bouachrine, *J. Saudi Chem. Soc.*, 21 (2017) 563.
35. Frisch, M. J.; Trucks, G. W.; Schlegel, H. B.; Scuseria, G. E.; Robb, M. A.; Cheeseman, J. R.; Montgomery, J. A.; Vreven, T.; Kudin, K. N.; Burant, J. C.; Millam, J. M.; Iyengar, S. S.; Tomasi, J.; Barone, V.; Mennucci, B.; Cossi, M.; Scalmani, G.; Rega, N.; Petersson, G. A.; Nakatsuji, H.; Hada, M.; Ehara, M.; Toyota, K.; Fukuda, R.; Hasegawa, J.; Ishida, M.; Nakajima, T.; Honda, Y.; Kitao, O.; Nakai, H.; Klene, M.; Li, X.; Knox, J. E.; Hratchian, H. P.; Cross, J. B.; Adamo, C.; Jaramillo, J.; Gomperts, R.; Stratmann, R. E.; Yazyev, O.; Austin, A. J.; Cammi, R.; Pomelli, C.; Ochterski, J. W.; Ayala, P. Y.; Morokuma, K.; Voth, G. A.; Salvador, P.; Dannenberg, J. J.; Zakrzewski, V. G.; Dapprich, S.; Daniels, A. D.; Strain, M. C.; Farkas, O.; Malick, D. K.; Rabuck, A. D.; Raghavachari, K.; Foresman, J. B.; Ortiz, J. V.; Cui, Q.; Baboul, A. G.; Clifford, S.; Cioslowski, J.; Stefanov, B. B.; Liu, G.; Liashenko, A.; Piskorz, P.; Komaromi, I.; Martin, R. L.; Fox, D. J.; Keith, T.; Al-Laham, M. A.; Peng, C. Y.; Nanayakkara, A.; Challacombe, M.; Gill, P. M. W.; Johnson, B.; Chen, W.; Wong, M. W.; Gonzalez, C.; Pople, J. A. GAUSSIAN 09, Gaussian, Inc., Pittsburgh, PA, (2009).
36. S. A. Halim and A. K. Khalil, *J. Mol. Struct.*, 1147 (2017) 651.
37. G. L. F. Mendonça, S. N. Costa, V. N. Freire, P. N. S. Casciano, A. N. Correia, and P. de Lima-Neto, *Corros. Sci.*, 115 (2017) 41.
38. S. Kaya, C. Kaya, L. Guo, F. Kandemirli, B. Tüzün, İ. Uğurlu, L. H. Madkour, M. Saraçoğlu, *J. Mol. Liq.*, 219 (2016) 497.
39. Y. Sasikumar, A. S. Adekunle, L. O. Olasunkanmi, I. Bahadur, R. Baskar, M. M. Kabanda, I. B. Obot, E. E. Ebenso, *J. Mol. Liq.*, 211 (2015) 105.
40. BIOVIA Materials Studio version 8.0, Accelrys USA, (2014).

41. M. Shahraki, M. Dehdab, and S. Elmi, *J. Taiwan Inst. Chem. Eng.*, 000 (2016) 1.
42. O. A. Dabar, Etude des processus de corrosion du nickel par dynamique moléculaire avec un potentiel réactif ReaxFF, thesis, University 'Bourgogne', France, 2012.
43. A. Singh, K.R. Ansari, J. Haque, P. Dohare, H. Lgaz, R. Salghi, M.A. Quraishi, *J. Taiwan Inst Chem Eng*, 82 (2018) 233.
44. Y. Sasikumar, A.S. Adekunle, L.O. Olasunkanmi, I. Bahadur, R. Baskar, M.M. Kabanda, I.B. Obot, E. E. Ebenso, *J. Mol. Liq.* 211 (2015) 105.
45. C. Verma, M.A. Quraishi, A. Singh, *J. Taiwan. Inst. Chem. Eng.* 49 (2015) 229.
46. A. Dutta, S. Saha, U. Adhikari, P. Banerjee and D. Sukul, *Corros. Sci.*, 123 (2017) 256.
47. H. Behzadi, P. Roonasi, M.J. Momenib, S. Manzetti, M.D. Esrafil, I.B. Obote, M. Yousefvand, S. M. Mousavi-Khoshdel b, *J. Mol. Struct.*, 1086 (2015) 64.
48. I.O. Ali, A.I. Hanafy, T.M. Salama, K.S. El-Nasser, A.A. El-Henawy, H.A. Guma, H.M. Mohamed, *Microporous and Mesoporous Materials*, 262 (2018) 35.
49. A. Singh, K.R. Ansari, K. Ashok, W. Liu, C. Songsong, Y. Lin, *J. Alloys and Compounds* 712 (2017) 121.
50. M. Goyal, S. Kumar, I. Bahadur, C. Verma, E.E. Ebenso, *Journal of Molecular Liquids*, 256 (2018) 256.
51. A. Y. Musa, A. Amir, H. Kadhum, A. B. Mohamad, A. Ahmad, B. Rahoma, H. Mesmari, *J. Mol. Str.* 969 (2010) 233.
52. Sudheer, M. A. Quraishi, *Ind. Eng. Chem. Res.* 53 (2014) 2851.
53. L. Guo, S. Z. Safi, S. Kaya, W. Shi, B. Tüzün, N. Altunay and C. Kaya, *Frontiers in chemistry*, 6 (2018) 155.
54. M. Raja, R. Raj Muhamed, S. Muthu, and M. Suresh, *J. Mol. Struct.*, 1141 (2017) 284.
55. L. Boucherit, T. Douadi, N. Chafai, M. Al-Noaimi, S. Chafaa, *Int. J. Electrochem. Sci.*, 13 (2018) 3997.
56. D.O. Isin, N. Karakus, *Journal of the Taiwan Institute of Chemical Engineers* 50 (2015) 306.
57. I.B. Obot, E.E. Ebenso, M.M. Kabanda, *Journal of Environmental Chemical Engineering* 1 (2013) 431
58. M. M. Kabanda, L. C. Murulana, M. Ozcan, F. Karadag, I. Dehri, I.B. Obot, E. E. Ebenso, *Int. J. Electrochem. Sci*, 7 (2012) 5035.
59. M. M. Kabanda, L. C. Murulana, E. E. Ebenso, *Int. J. Electrochem. Sci*, 7 (2012) 7179.
60. E. E. Ebenso, M. M. Kabanda, T. Arslan, M. Saracoglu, F. Kandemirli, L. C. Murulana, A. K. Singh, S. K. Shukla, B. Hammouti, K.F. Khaled, M.A. Quraishi, I.B. Obot, N.O. Eddy, *Int. J. Electrochem. Sci*, 7 (2012) 5643.
61. H. Behzadi, P. Roonasi, M. J. Momeni, S. Manzetti, M. D. Esrafil, I.B. Obot, M. Yousefvand, S. M. Mousavi-Khoshdel, *Journal of Molecular Structure* 1086 (2015) 64.
62. D. Turcio-Ortega, T. Pandiyan, J. Cruz, E. Garcia-Ochoa, *J. Phys. Chem. C*, 111 (2007) 9853.